Review Article

Quantitative magnetic resonance imaging in Alzheimer's disease: a narrative review

Bhavsimran Singh Malhi[1]^, James Lo[1,2], Marco Toto-Brocchi[1], Atlas Haddadi Avval[3], Yajun Ma[1], Jiang Du[1]

[1]Department of Radiology, University of California, San Diego, La Jolla, CA, USA; [2]Department of Bioengineering, University of California, San Diego, La Jolla, CA, USA; [3]School of Medicine, University of Medical Sciences, Mashhad, Iran

Contributions: (I) Conception and design: BS Malhi, Y Ma, J Du; (II) Administrative support: Y Ma, J Du; (III) Provision of study materials or patients: BS Malhi, Y Ma, J Du; (IV) Collection and assembly of data: All authors; (V) Data analysis and interpretation: None; (VI) Manuscript writing: All authors; (VII) Final approval of manuscript: All authors.

Correspondence to: Jiang Du, PhD. Department of Radiology, University of California, San Diego, 9500 Gilman Drive, La Jolla, CA 92093, USA. Email: jiangdu@health.ucsd.edu.

Background and Objective: Alzheimer's disease (AD) is a complex neurodegenerative disorder characterized by progressive cognitive decline and is traditionally associated with grey matter pathology. Recent research highlights the significance of white matter and myelin damage in AD, presenting a paradigm shift in understanding the disease. The aim of this study was to summarize current advancements in magnetic resonance imaging (MRI) techniques and their applications in assessing myelin and brain pathology in AD with a special focus on ultrashort echo time (UTE) based techniques, alongside the role of artificial intelligence (AI) in enhancing diagnostic accuracy.

Methods: Between April and May 2024, we conducted a literature search using Google Scholar, Web of Science, and PubMed, focusing on publications from 1990 to 2024. Search terms included "Quantitative imaging", "Alzheimer's MRI", "T1ρ Alzheimer's", "MT imaging Alzheimer's", and "myelin water fraction Alzheimer's". We included quantitative MRI studies involving AD brains and excluded volumetric analyses, non-quantitative studies, non-English reports, non-peer-reviewed studies, and animal research.

Key Content and Findings: Quantitative MRI techniques, including T1, T1ρ, magnetization transfer ratio (MTR), T2, T2*, susceptibility, myelin water fraction (MWF), and non-aqueous myelin proton density (PD) were described. These biomarkers represent different pathophysiological elements of brain damage and may have distinct functions at different phases of the disease. The role of AI in enhancing diagnostic accuracy is also discussed.

Conclusions: In conclusion, integrating advanced MRI techniques and AI offers promising avenues for understanding and diagnosing AD. The focus on myelin damage and white matter integrity underscores the importance of comprehensive imaging approaches. Continued research and development are essential to address current challenges and improve clinical practice in AD diagnostics.

Keywords: Quantitative analysis; magnetic resonance imaging (MRI); white matter (WM); myelin; Alzheimer's disease (AD)

Submitted Aug 11, 2024. Accepted for publication Feb 25, 2025. Published online Mar 28, 2025.
doi: 10.21037/qims-24-1602
View this article at: https://dx.doi.org/10.21037/qims-24-1602

^ ORCID: 0000-0003-0347-0983.

© AME Publishing Company.

Introduction

Alzheimer's disease (AD) presents one of the most significant challenges in global health, being the leading cause of dementia in the elderly population (1). Worldwide, AD accounts for 60–80% of all cases of dementia (2,3). In the US, the number of people over 65 years of age affected by Alzheimer's dementia is estimated at around 6.7 million (2), significantly impacting patients' lives, their families and the healthcare system as a whole. It is projected that by 2060, the number of people over 65 years of age with Alzheimer's dementia will reach 13.8 million (4). AD typically results in a prolonged illness characterized by severe disability and dependence, further contributing to the public health impact of the disease. The global impact of AD is becoming progressively more relevant due to the worldwide population aging, making it a crucial field for research. For this reason, the interest in AD research keeps growing, with the Funding for AD, including AD related dementias (ADRD), almost reaching 4 billion dollars in 2023 (5).

The clinical diagnosis of AD is an intricate process that involves various factors, including the patient's medical history, clinical tests, neuroimaging, and biomarkers. However, a fully certain diagnosis is challenging due to the numerous co-morbidities often linked with dementia, such as cerebrovascular disease, cerebral amyloid angiopathy, hippocampal sclerosis (HS), and other region-specific findings (6,7). Additionally, the presence of different pathologies associated with other dementias, such as Lewy body dementia, further complicates the diagnosis. Therefore, the variability of the clinical conditions associated with AD can make clinical diagnosis extremely challenging, especially in the early phases, showing a low concordance with post-mortem pathological assessment (8). A definitive diagnosis of AD can be established only post-mortem, by looking for Beta-amyloid plaques, neurofibrillary tangles (NFTs) and neuritic plaques (9,10).

While AD has traditionally been regarded as a grey matter (GM) disorder, studies have indicated that myelin damage is a central feature in AD and may even precede the development of Aβ and tau pathologies (11-13). Myelin damage has been found to occur prior to the deposition of Aβ plaques and NFTs in the brains of murine models of AD (14,15). One recent study by Couttas *et al.* (13) revealed a defect in ceramide synthase 2 activity—an enzyme involved the biosynthesis of myelin lipids in the preclinical stages of the disease, e.g., Braak stage I/II within the temporal cortex, which suggests that myelin dysfunction precedes amyloid pathology. There is also evidence that tau protein hyperphosphorylation may occur later, during the remyelination process (16).

The relationship between white matter (WM) and GM changes has been extensively investigated. Myelin basic protein (MBP), which is a structural protein component of myelin, has been proven to have a regulating role in the deposition of Aβ 42 by preventing the formation of amyloid plaques in the brain (17,18). On the other hand, the deposition of Aβ has been shown to induce oligodendrocyte death and inhibit myelin formation (19-21). There is a strong association between decreased MBP levels and increased Aβ in the brain tissue of AD patients (22).

Neuroimaging, particularly magnetic resonance imaging (MRI), serves as a crucial tool for *in vivo* diagnosis. It enables clinicians to make an early diagnosis and choose the most appropriate therapeutic path to prevent or delay cognitive decline. The literature widely supports the pivotal role of clinical MRI (with a magnetic field between 1.5 T and 3 T) in detecting most pathological changes related to AD before the patient's death, showing high sensitivity and moderate specificity (8,23).

Cerebral atrophy in the antemortem brain appears to be the strongest indicator of underlying AD neuropathology along with other incidental neurodegenerative findings such as HS and TDP-43 encephalopathy (8,24). White matter hyperintensity (WMH), on the other hand, exhibits a better correlation with concomitant cerebrovascular disease observed at autopsy (8). International guidelines recommend using MRI in the clinical context for patients with dementia and mild cognitive impairment (MCI) to rule out reversible brain abnormalities, such as tumors or subdural hematomas (25). MRI can also occasionally provide important information concerning vascular pathology or the pattern of cortical atrophy (26). Positron emission tomography (PET) has shown higher specificity than MRI, but MRI is cheaper and noninvasive, which makes it a desirable substitute for nuclear medicine (27). A recent study involving patients with cognitive impairment and AD has shown associations between brain MRI phenotypes and single nucleotide polymorphisms (SNPs) (28).

Diffuse atrophy is the main MRI feature in AD, with the entorhinal cortex and the hippocampus being the two most common regions of interest in both *in vivo* and post-mortem investigations into AD pathophysiology (29). Although its ability to predict cognitive deterioration in MCI patients either alone or in conjunction with other metrics is still being explored, structural MRI might not have enough specificity to distinguish AD from other disorders (30). However, a visual qualitative assessment of MRI is insufficient to estimate the rate of tissue loss in affected areas, necessitating quantitative measures for accurate

© AME Publishing Company.

Table 1 Search strategy summary

Items	Specification
Data search performed	April to May 2024
Databases searched	Google Scholar, Web of Science, PubMed
Search terms used	Quantitative imaging, Alzheimer's MRI, T1ρ Alzheimer's, MT imaging Alzheimer's, myelin water fraction Alzheimer's
Timeframe	1990 to 2024
Inclusion and exclusion criteria	Quantitative MRI studies involving AD brains were included
	Non quantitative studies, volumetric analyses, non-English language reports, non-peer reviewed studies, animal studies were excluded
Selection process	The literature search and selection were conducted by B.S.M., and the selection process was discussed by all authors. Differences were resolved by consensus

assessment. Additionally, the human eye cannot perceive the minimum degree of atrophy, and without quantitative measurements, image evaluation becomes subjective (29).

Although hippocampal volumetry is the most widely studied structural MRI biomarker of AD (31), recent studies suggest texture analysis has advantages over volume and shape approaches, and it may be used to detect microstructural changes earlier with better accuracy (32-34).

In recent decades, quantitative MRI (qMRI) has revolutionized neuroimaging, providing a detailed and advanced approach to studying AD. It allows for the investigation of the complex and subtle changes in the brain involved in the AD pathogenetic process, leading to improvements in diagnosis, follow-up, and the identification of new therapeutic targets. In this review, we aim to summarise the qMRI techniques which can noninvasively measure a variety of parameters, including T1, T1ρ, T2, T2*, susceptibility, magnetization transfer ratio (MTR), myelin water fraction (MWF), and non-aqueous myelin proton density (PD), which are thought to represent different pathophysiological elements of brain damage and may have distinct functions at different phases of the disease. Moreover, these parameters, being quantitative, are useful for statistical comparisons and longitudinal studies, offering the opportunity to analyze a vast amount of new data. We present this article in accordance with the Narrative Review reporting checklist (available at https://qims.amegroups.com/article/view/10.21037/qims-24-1602/rc).

Methods

This review conducted between April and May 2024 aimed to provide a thorough description of the current qMRI studies in AD. The literature search was performed in PubMed, Web of Science, and Google Scholar databases for studies published between 1990 to 2024. The results were screened first automatically and then through title and abstract reading to exclude non quantitative studies, volumetric analyses, non-English language reports, non-peer reviewed studies and animal studies. *Table 1* summarises the search strategy.

Discussion

T1

T1 relaxation time is also known as spin-lattice relaxation or longitudinal relaxation time, which characterizes how quickly the longitudinal magnetization (M_z) recovers back to 63% of its initial value after rotation into the transverse plane. T1 relaxation time changes are related to water content, amyloid burden, iron load, and myelin loss, among other factors; hence, inconsistent T1 results have been reported in AD patients (35-37).

Gouw *et al.* (38) performed a histologically correlated study on *ex-vivo* brain samples using a 3D fast low-angle shot (FLASH) for T1 quantification of WM. In AD brain samples, both normal-appearing white matter (NAWM) and WMH exhibited higher T1 values compared to control samples for NAWM and WMH, respectively. The difference between T1 of NAWM and WMH was higher in AD brains than in controls. These changes were likely due to microglial activation, which was demonstrated pathologically and is an independent factor causing T1 increase. The T1 times were also independently related to axonal loss and myelin loss.

© AME Publishing Company.

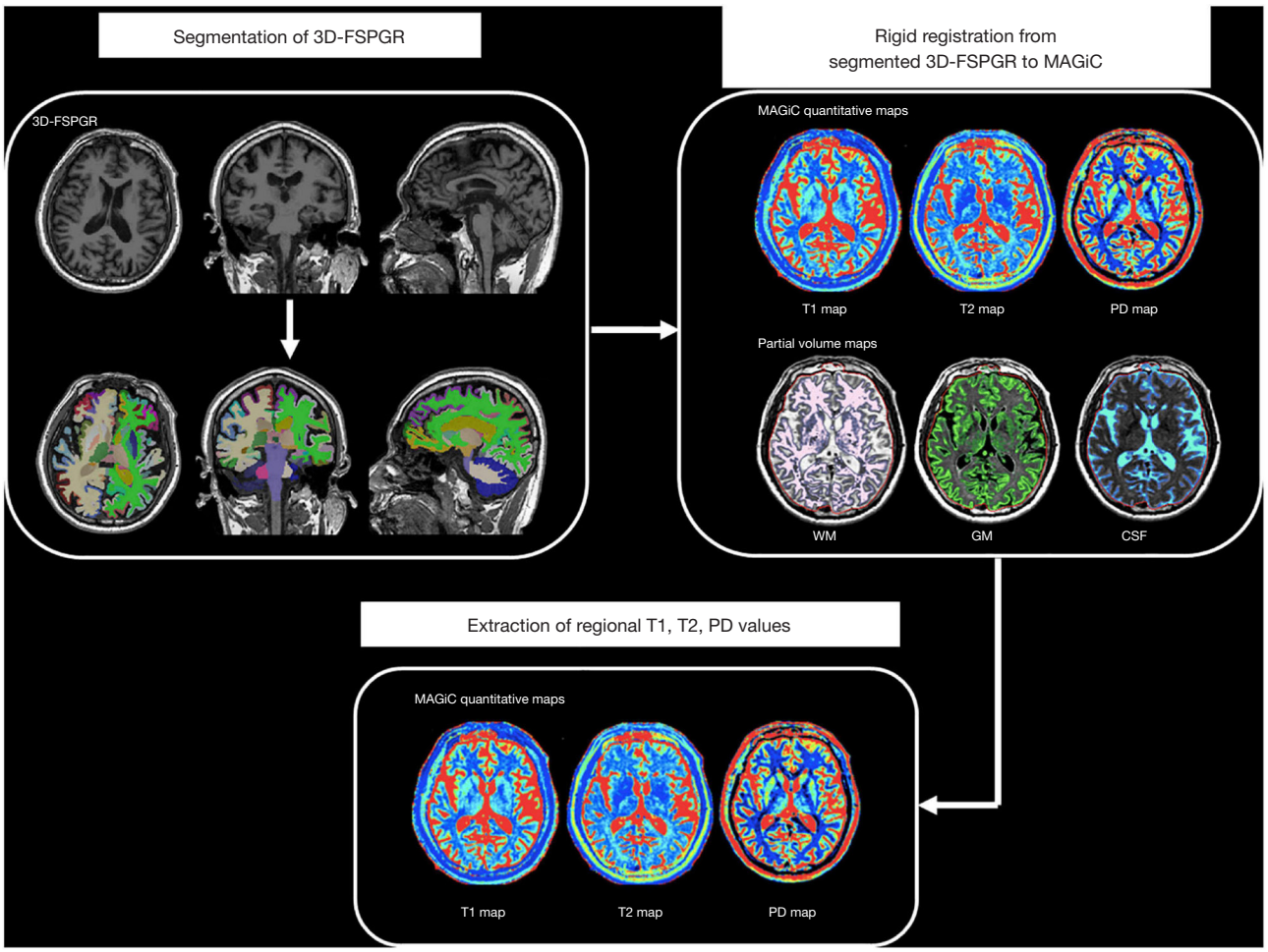

Figure 1 Schematic diagram of post-processing and measurements of synthetic MRI data. To obtain brain regional relaxation values, parcelation in subject's native space using FreeSurfer1 with Destrieux atlas (41) based on the 3D-FSPGR images was performed. After rigid registration between 3D-FSPGR and synthetic MRI images using MATLAB R2016a (MathWorks, Natick, MA, USA) and SPM12 brain regional T1, T2, and PD values were extracted. The figure was reused from an open access article (40), under the terms of the Creative Commons Attribution License 4.0 (CCBY). 3D-FSPGR, 3 dimensional fast spoiled gradient recalled echo; CSF, cerebrospinal fluid; GM, grey matter; MAGiC, magnetic resonance image compilation; MRI, magnetic resonance imaging; PD, Parkinson's disease; WM, white matter.

Su *et al.* (39) used an inversion recovery based echo planar imaging (EPI) sequence to study GM changes in AD. They found a reduction in T1 values in bilateral temporal and parietal lobes, hippocampus, and basal ganglia. The T1 values in the AD group increased over the 12-month follow-up period. Lou *et al.* (40), on the other hand, used a novel synthetic MRI sequence and found similar results for the caudate nucleus but increased T1 values in the right insular cortex. *Figure 1* illustrates the steps involved in the post-processing and measurement (40,41) of synthetic MRI data. A recent study by Parent *et al.* (42) argued that T1 was not a sensitive measure of microstructural tissue alterations and its clinical relevance was limited. However, these studies were conducted with limited sample sizes, emphasizing the need for additional research to provide a clearer understanding.

T1

T1ρ relaxation time describes spin-lattice relaxation in the rotation frame in the presence of an external radio frequency (RF) pulse (also called spin-lock pulse), which

© AME Publishing Company.

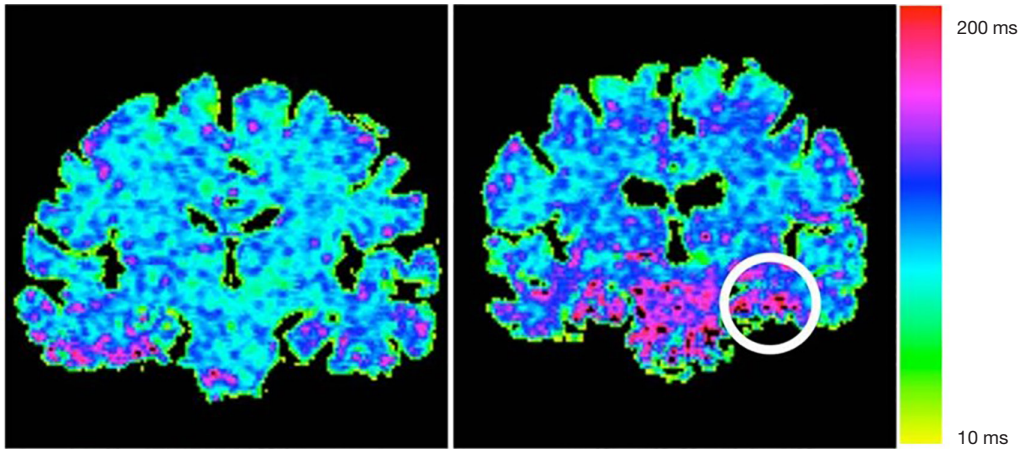

Figure 2 T1ρ maps of brain of control (61-year-old female) and AD (57-year-old female) brain. Pixels with higher T1ρ are more prominent in AD patients especially in the medial temporal lobe region as indicated by the white circle on the 57-year-old AD patient. The absence of T1ρ signal from CSF indicates that the higher T1ρ values are not due to fluid. This figure was reused from (45) with permission. AD, Alzheimer's disease; CSF, cerebrospinal fluid.

is applied along the magnetization after RF excitation. The spins are considered stationary relative to this external RF field in the rotating frame and undergo slower relaxation than T2 but faster than T1. T1ρ is sensitive to low frequency motional processes (100 Hz to a few kHz) and provides useful information about macromolecular composition, which is not directly studied by T1 and T2 imaging (43). T1ρ displays a greater range of values than T2 in the human brain (44).

Borthakur *et al.* compared the medial temporal lobe region of AD and control brains and found increased T1ρ relaxation times for white and GM (45). The same group also reported 10% higher T1ρ values in the hippocampus of patients with AD as compared to age-matched controls (46). *Figure 2* compares T1ρ maps in the brain of a healthy volunteer and an AD patient. Combining T1ρ with cerebrospinal fluid (CSF) biomarkers like T-tau, P-tau, and Aβ-42 improves the prediction rate for AD and MCI. Compared to CSF markers (77%), T1ρ showed higher sensitivity (82%) in delineating AD from controls (47).

Another unique feature of T1ρ MRI is its sensitivity to pH (48-51). Multiple studies have demonstrated that higher T1ρ relaxation times indicate a lower pH, signifying increased acidity. The pathological cascades associated with the development of AD, like vasculopathy, amyloid pathology, tau pathology, metabolic disturbances, oxidative stress, etc, have a common element: acidosis. T1ρ, thus could possibly serve as a biomarker reflecting a composite picture of the different pathologies involved. In their study, Boles Ponto *et al.* found that a higher global T1ρ was associated with amyloid burden, abnormal cerebral glucose metabolism, and poor memory and cognitive function (52).

Various factors, including field inhomogeneities, influence quantitative imaging, and it is imperative to minimize image artifacts to ensure accurate quantification. In a recent study by Wang *et al.* (53), high test-retest repeatability for T1ρ measurements in the human brain *in vivo* was demonstrated, which suggests that T1ρ may be a reliable technique for quantitative brain analyses within clinically relevant scan times. However, it is important to note that the study involved a moderate-sized cohort of 30 patients and utilized a spin lock frequency of 300 Hz, as opposed to the more commonly used 500 Hz. As a result, further research is necessary to validate and assess the repeatability of T1ρ techniques.

T2

T2 relaxation time is also known as spin-spin relaxation or transverse relaxation time. It characterizes how quickly the transverse magnetization (M_{xy}) decays to 37% of its initial value in the magnetic resonance system. Quantitative T2 relaxometry analysis was one of the earliest approaches to studying AD quantitatively.

Multiple studies have found increased T2 values in the hippocampus (54-58). The hippocampus is the site of early pathological changes in AD (59). It is closely associated

© AME Publishing Company.

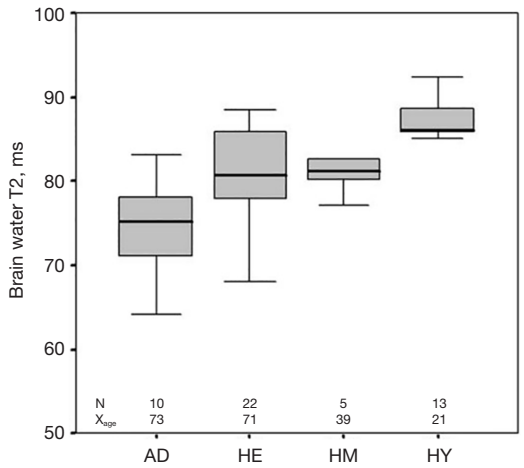

Figure 3 Box-and-whiskers plot of hippocampal T2 relaxation times using magnetic resonance spectroscopy. T2 values decreased with age and AD (whiskers mark the outermost value within 2.5 SDs). The figure was reused from (61) with permission. AD, Alzheimer's disease; HE, healthy elderly adults; HM, healthy middle-aged adults; HY, healthy young adults; SD, standard deviation; N, sample size; X_{age}, mean age.

with cognitive functions in the brain, including memory and neurogenesis. Neuropathological abnormalities in AD include neuronal loss and gliosis in the hippocampus (12). The major pathophysiological changes described in AD are the accumulation of amyloid beta, phosphorylated tau, and neuroinflammation. The neurodegeneration starts in the entorhinal cortex of the hippocampal formation and gradually extends into the temporal cortex, frontoparietal cortex, and subcortical nuclei (60). Over time, this leads to disruptions in the normal brain pathways responsible for learning and memory deficits. The increase in T2 can be explained by multiple pathological changes in AD, namely loss of pyramidal neurons, gliosis or glioma, and increased CSF in the atrophied region. However, early quantitative T2 studies used mono-exponential analysis to study the region, assuming a CSF-free pixel. This assumption may not be valid in populations with cerebral atrophy, such as healthy elderly and AD patients, where CSF constitutes a more significant portion of the total intracranial volume. Even if appearing to contain only tissue, the pixel may have a small but significant CSF signal component. Haley *et al.* (61) performed a biexponential spectroscopic T2 analysis to separate the tissue (hippocampus) and CSF signals to better study the effect of AD on T2 values in the hippocampus. They reported a shortening of T2 values with age and AD, as shown in *Figure 3*. Subsequent studies by other groups have reported similar findings (36,39,62). The reported increase in T2 in the older studies was probably due to the presence of CSF, which led to signal averaging of tissue and CSF T2 values, resulting in greater T2 values than true brain tissue. However, it is also well known that AD is associated with iron accumulation (63-65). Tissue iron accumulation is associated with extracellular amyloid plaques (66-68) and intracellular NFTs (69,70). Schenck *et al.* (71) performed an iron extraction study in which they measured T2 values in the hippocampus before and after iron extraction and found a global increase in T2 values in the brain, including the hippocampus. Therefore, it is these two competing factors, the mobile water component and the iron, that determine T2 values in the hippocampus.

Susceptibility

Magnetic susceptibility is a macroscopic physical property that describes the tissue's own magnetization when placed in an external magnetic field. The magnetic susceptibility of brain tissue is dominated by four major constituents: water, myelin, iron and calcium (72). Diamagnetic myelin and paramagnetic iron are the dominant sources of susceptibility contrast. Myelin is the insulating sheath surrounding nerves in the brain and spinal cord. It is composed of about 40% water, and the dry mass comprises 80% lipids and 20% protein. The lipids and proteins in the myelin sheath are major contributors to its diamagnetic susceptibility. Iron in the brain is regulated by iron regulatory proteins (IRPs)—transferrin (Tf), transferrin receptor 1 (TfR1), ferritin, ferroportin 1 (FPN1), divalent metal transporter 1 (DMT1), etc. (73). In addition to these proteins, APP and tau also act to regulate iron. APP interacts with FPN to regulate the efflux of ferrous ions (74). APP knockout mice show increased levels of iron deposition and oxidative stress in cortical neurons (75). Tau functions as an intracellular microtubule-associated protein, facilitating the transportation of the produced APP to the cell surface, thereby promoting iron output (76). Notably, mice lacking tau exhibit age-dependent iron accumulation and brain atrophy. Additionally, the reduced surface trafficking of APP in primary cultured neurons leads to iron retention, suggesting that tau-mediated iron homeostasis might depend on APP (77,78).

Another key factor, recently explored in more detail, is the permeability of the blood-brain barrier (BBB). Through BBB imaging, researchers have found that increased BBB permeability may contribute to higher iron and Aβ accumulation in the brains of individuals with

© AME Publishing Company.

Alzheimer's (79). Uchida *et al.* (80) in their study on iron deposition in brain measured using quantitative susceptibility mapping (QSM) and BBB function measured using diffusion-prepared pseudo-continuous arterial spin labeling were able to demonstrate relationship between brain iron dynamics and BBB function in children. Also in another study, Uchida *et al.* (81) found that increased APO *ε4* dose (*APOE ε4* non-carriers>heterozygotes>homo zygotes) is associated with decreased effective brain-waste clearance, such as iron and β-amyloid, through the BBB.

When compared to traditional contrast weightings, T2* mapping, and susceptibility weighted imaging (SWI), QSM provides a superior contrast to noise ratio (CNR) and quantitative measurement of iron and myelin without dependence on orientation and non-local effects (82). Iron accumulation increases R2* and QSM. Breakdown of intact myelin decreases R2* but does not change QSM, whereas degradation and removal of myelin increase susceptibility measured on QSM. QSM values do not represent absolute magnetic susceptibilities and must be interpreted as a relative measure that must be normalized to a reference region.

Acosta-Cabronero *et al.* (83) first described a complete framework for magnetic susceptibility measurements in AD patients and found increased QSM in the putamen of patients compared to controls. The statistical effect of QSM data in separating AD from controls in the putamen was as strong as that of hippocampal atrophy. This study, although having a small sample size, demonstrated the potential of QSM as an MRI biomarker. QSM can be used to differentiate AD from healthy controls (84) as well as MCI from AD (85). Gong *et al.* successfully showcased the diamagnetic properties of Amyloid beta and tau proteins through both phantom and *ex vivo* experiments. The negative susceptibility map for beta-amyloid and tau, contrasting with the positive susceptibility of iron, offers a histology-like image contrast (86). Nevertheless, the co-localization of iron and beta-amyloid may introduce contrasting effects on QSM maps. Furthermore, the limited ability of clinical MRI to achieve the ultra-high resolution utilized in this study diminishes the specificity of susceptibility maps when employed as a tool for macromolecular quantification in clinical settings. Cogswell *et al.* (87), in their study on a relatively larger sample size, found increased susceptibilities in deep and inferior gray nuclei-pallidum, putamen, substantia nigra, and subthalamic nucleus. Higher susceptibility was significantly associated with higher amyloid PET standardized uptake value ratio (SUVr) in the pallidum and putamen and higher tau PET in the basal ganglia, which had the largest effect size in the pallidum. The cortical regions did not consistently show disease related changes in QSM. The iron levels associated with cortical amyloid plaque and neurodegeneration were of insufficient quantity to be detected *in vivo* with QSM, or there may be local factors, including amyloid deposition, counteracting the anticipated susceptibility changes from local iron deposition. The greater effect sizes in the deep and inferior nuclei were likely based on the greater dynamic range in these regions. *Figure 4* shows comparison of QSM and histological stainings of amyloid-β, tau, and iron in the frontal cortex of a control and AD patient.

MTR

Magnetization transfer (MT) refers to the transfer of spin magnetization from macromolecular protons to water protons. In MT imaging, a saturation pulse is placed at a frequency offset Δf) away from the water peak to saturate macromolecular protons, which exchange with water protons via chemical exchange or MT, significantly reducing the detectable signal. A simple way to quantify the MT effect is to measure MTR, which has been used for indirect assessment of macromolecules with restricted motion and extremely short T_2s.

MTR has been employed for noninvasive evaluation of many neurological diseases including AD. Hanyu and colleagues initially examined the hippocampus in dementia patients using MTR (88). They found that MTR measurements could offer greater specificity than visual analysis in identifying structural impairment of the hippocampus in individuals with AD. The mean MTR levels in the hippocampus and temporal lobes have been found to be reduced in AD brains compared to those in control brains (88-90).

Apart from the mean MTR values, an MTR histogram analysis has been used to better characterize the changes in WM. Measures like 'peak position,' the MTR value with the highest frequency, and the 'relative peak height,' the relative voxel count at the peak position, have been defined. Relative peak height indicates parenchymal damage and is unaffected by brain atrophy. Results from MTR histogram analyses have even suggested that mean MTR changes are not restricted to the temporal lobes but can be found more globally throughout the brain (91-93). In their work, Ridha *et al.* assessed the value of measuring both MTR and brain volumes in differentiating patients with AD from control subjects. They found that using both parameters (brain volume and mean MTR) in combination provided significantly higher sensitivity in differentiating AD patients from controls than either parameter alone (93).

© AME Publishing Company.

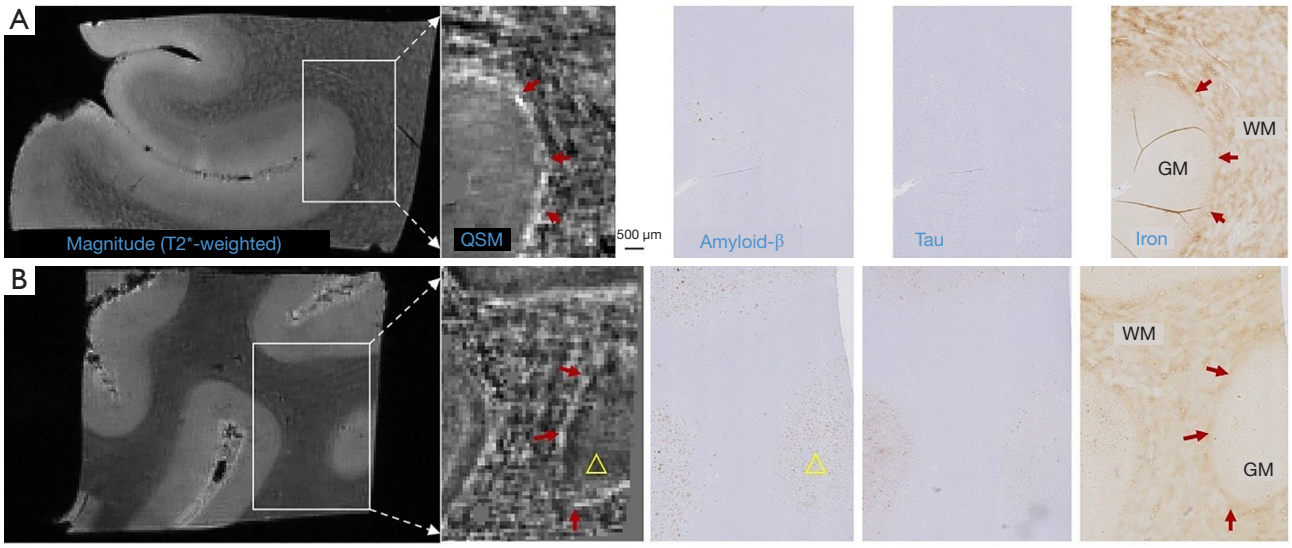

Figure 4 Comparison of QSM and histological stainings of amyloid-β, tau, and iron in the frontal cortex of a control (A) and AD patient (B). (A) Control: QSM shows hyper-intense paramagnetic susceptibility at gray-white matter boundaries that match the iron staining (red arrows). Cortical gray matter shows low staining for amyloid-β, tau, and iron and has a susceptibility near zero. (B) AD patient: QSM shows hyper-intense paramagnetic susceptibility at the gray-white matter boundaries that match the iron staining (red arrows). One cortical gray matter region shows moderate amyloid-β staining (yellow triangle) and low tau staining, which has diamagnetic susceptibility. The figure was reused from (86) with permission. AD, Alzheimer's disease; GM, grey matter; QSM, quantitative susceptibility mapping; WM, white matter.

Ropele *et al.* (94) studied the longitudinal MTR changes in patients with AD. They found that AD patients had significantly and consistently lower global MTR values through the one-year follow-up period. Deep brain nuclei like the thalamus, putamen, and caudate nucleus showed significant reductions in MTR at 12 months follow-up compared to baseline. Furthermore, these findings were complemented by correlations with the mini-mental state examination (MMSE), suggesting the role of deep GM structures in the pathogenesis of AD (95-98).

In brain regions most susceptible to damage in AD, U-fibers in the superficial WM appear to be the most vulnerable type of neurons. In their study, Fornari *et al.* (99) demonstrated a widespread reduction in MTR values in superficial WM with predominant involvement of the left hemisphere, as in previous studies (34,45). They also demonstrated two distinct patterns of demyelination in surface WM based on the age of AD onset, underlining the potential of MTR imaging as an *in vivo* biomarker superior to currently used techniques. *Figure 5* shows widespread decrease in MTR values in different regions of the brain.

MTR, however, is affected by various factors like RF excitation amplitude, frequency offset, duty cycle, acquisition parameters, and tissue properties. It is therefore more desirable to measure the voxel-level MT-related intrinsic tissue properties, e.g., the forward magnetization transfer rate (k_{for}) map from tissue water to macromolecular protons, independent of the data acquisition details. Lower k_{for} values have been reported in multiple brain grey and WM regions (100,101). These studies, however, analyzed predetermined regions of interest for increased signal-to-noise ratio (SNR). Recently, Duan *et al.* (102) demonstrated voxel-wise k_{for} abnormalities in AD, enabling precise detection of abnormal k_{for} values in spatial locations associated with AD, without predefined hypotheses.

Another intrinsic MT parameter that is studied is the macromolecular fraction (MMF). In biological tissues, macromolecules such as proteins and lipids have restricted molecular motion compared to free water molecules. The MT process involves the exchange of magnetization between these two compartments. The MMF is a quantitative measure of the total magnetization fraction associated with macromolecules. MMF has been studied in tissues like meniscus (103), cartilage (104,105), brain (106,107), tendon (108,109), etc. This MMF or myelin proton fraction is not affected by the spatial orientation of myelinated fibers (affects diffusion imaging indexes) (110-113),

© AME Publishing Company.

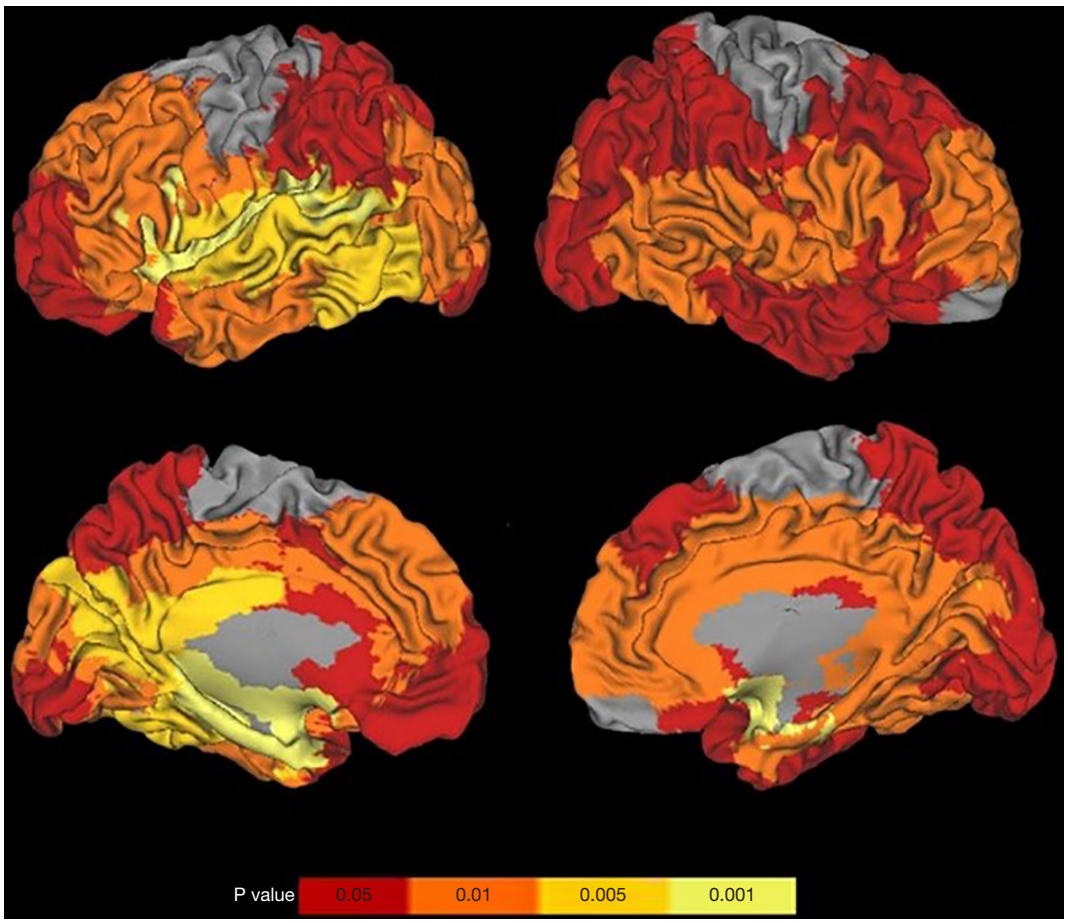

Figure 5 The results of the 2-sample *t* test for mean MTR values show a global decrease in MTR values in AD patients when compared to elderly controls. Each ROI has been tested separately and the results are displayed in a 3D rendering. They are thresholded at P<0.05 corrected for multiple comparisons. The color bar represents $P_{corrected}$ values. The figure was reused from (99), with permission. AD, Alzheimer's disease; MTR, magnetization transfer ratio; ROI, region of interest.

the concentration of iron and other paramagnetic ions (affects T1, T2, T2* quantification), and magnetic field strength (114,115). Kiefer *et al.* (116), in their study on qMT in the hippocampus, were able to distinguish MCI and AD brains using MMF and T2r (T2 of the restricted pool), whereas MTR could only distinguish control and AD brains. Studies have also shown reduced MMF in the right parahippocampal cingulum (117) and left thalamus (118) in asymptomatic participants with familial and genetic risk factors of AD.

MWF

While myelin is defined as the lipid layers that wrap concentrically around axons, myelin water (MW) is defined as the water trapped within these layers. In qMRI, MW is a target as an indirect measure of myelin content in the brain. However, like myelin, MW content is traditionally very difficult to image or quantify due to several factors. MW is localized within the very narrow gap (<4 nm) between myelin lipid layers, causing the water molecules to interact with neighboring lipids (119,120). Subsequently, it has unique signal characteristics as a hybrid between the very short T_2 relaxation times of macromolecules/non-aqueous myelin (<1 ms) from its tightly bound protons and the relatively long T_2 of intra/extracellular water (40–200 ms) and its more free protons. Furthermore, roughly ~70% of hydrogen atoms in WM are found in the intra/extracellular space, rendering the MW the nondominant signal source in this region (120). MW itself has a very short T_2 time between 10–20 ms, much shorter than that of intra/extracellular water and which decays

© AME Publishing Company.

rapidly on conventional MRI sequences. Simultaneously, the T_1 of MW is (<400 ms) and affected by the cross relaxation induced by the surrounding lipids (121). The resonance frequency of MW is also highly dependent on the specific orientation between WM fiber tracts and the B_0 field, namely when they are perpendicular, MW displays a large positive frequency shift, while intra/extracellular water displays a large negative shift.

Conventional MRI generally focuses on tissue with long T_2 water components such as the WM, GM, intra/extracellular water (40–200 ms), and CSF (>350 ms). This leaves out a critical biomarker that has the potential to be used in the broad evaluation of the brain as a whole.

As such, a variety of techniques have been developed to evaluate MW, specifically the MWF. MWF is typically defined as the ratio of the area of the MW T_2 distribution to the area of the entire T2 distribution. Many developed techniques have found that a reduced MWF is associated with myelin reduction and amyloid pathology in preclinical AD.

The Carr-Purcell-Meiboom-Gill (CPMG) T_2, or spin echo method utilizes a 90 ° excitation pulse followed by a series of 180° refocusing pulses to acquire a T_2 decay curve (122,123). The acquisitions can be accelerated by collecting multiple images per echo time using spiral acquisitions (122,124). To extract the shorter MW T_2 time from the total T_2 signal distribution of all brain tissue, non-negative least squares analysis (NNLS) was traditionally used and more recently, decomposing the decay curve into log-Gaussian components, namely CSF, intra/extracellular water, and MW (125,126). Decomposing into different components is generally considered more robust, but it may lead to misleading MWF results when the number of T2 components is underestimated or overestimated. Similar T_2 based MW techniques generally correlate well with myelin histology, even with region of interest (ROI) reproducibility, but suffer from poor voxel level reproducibility due to the inaccurate estimation (120,127). Multicomponent T_2 analysis and multicomponent-Driven Equilibrium Single Pulse Observation of T_1 and T_2 (mcDESPOT) model the brain tissue with two or more water components (typically MW and intra/extracellular water) and isolate them via postprocessing based on differences between the components' T_2/T_1. This is based on a spoiled gradient sequence and balanced free precession sequence. Visualization of short transverse relaxation time components (ViSTa) is based on acquiring multiple inversion recovery images with a wide range of T_1 for robust suppression of CSF and intra/extracellular water signals.

Studies have revealed a significant association between myelin loss, with its subsequent reduced MWF and AD state (128,129). *Figure 6* shows 3D T1 weighted images, MWF, grey matter volume (GMV), white matter volume (WMV) comparisons between a 72-year-old healthy female control and 73-year-old female AD patient. A decrease in the WMV and a gross signal drop in the MWF maps was observed in the AD patient. The largest area under curve (AUC) for differentiating between cognitively normal (CN) and AD groups was 0.79 in corpus callosum for MWF, 0,883 in hippocampus for gray matter volume (GMV) and 0.86 in hippocampus for WMV (128). This decreased MWF also follows cognitive impairment associated with aging, further implicating it as a useful biomarker for AD. Furthermore, reduced MWF is also related to positive apolipoprotein E4 (APOE4) status, a major genetic risk factor for AD, of which mutations are responsible for inhibiting amyloid β clearance and facilitating tau pathology (130).

Myelin PD

Myelin is a concentrically laminated membranous structure consisting of alternating protein and lipid layers, and is a major component of the WM of the brain. It is present in the form of a sheath surrounding the axons, insulating them from electrically charged ions and molecules. Myelin helps increase nerve conduction velocity. Loss of myelin is the hallmark of numerous inflammatory and neurodegenerative disorders, including multiple sclerosis (MS), AD, and other neurological diseases (131). Direct assessment of the integrity of myelin may be important. However, the non-aqueous myelin protons have extremely short T_2s (less than 1 ms), and cannot be directly imaged with conventional clinical MRI sequences which have TEs of several milliseconds or longer (132-137). As a result, conventional MRI sequences only provide an indirect assessment of myelin. Myelin-specific information, such as its T1 and T2* relaxation times and PD, is unknown. ultrashort echo time (UTE) sequences with minimum nominal TEs as short as 8 μs, which are more than 100 times shorter than the TEs of conventional MRI sequences, make it possible to directly detect signal from myelin using clinical whole-body scanners (132-142).

While UTE-type sequences with TEs <0.1 ms allow direct myelin imaging, the major challenge to this approach is selectivity because water components with longer T2 show far higher signals than myelin (143). Adiabatic inversion recovery (IR) pulses allow uniform inversion and suppression of the longitudinal magnetizations of various water components, making it possible to image myelin

© AME Publishing Company.

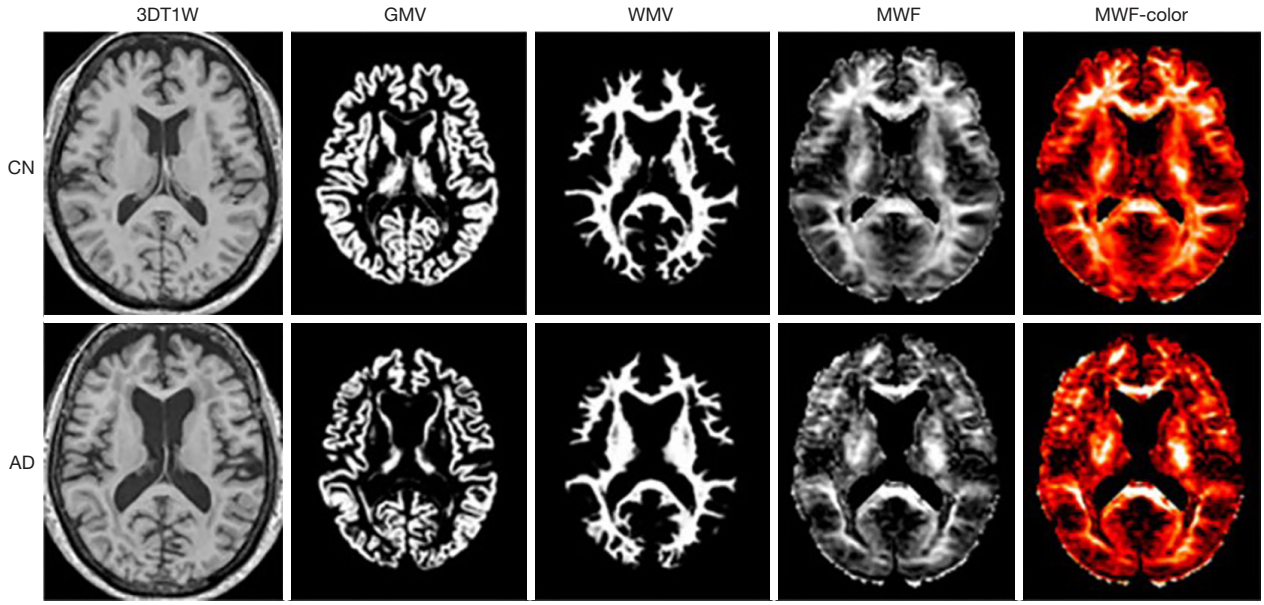

Figure 6 Representative maps of the 3D T1W, GMV, WMV and MWF with and without color code. A gross signal drop in the apparent MWF signal was observed in the AD group compared to the CN group in the white matter. This figure was adapted from an open access article (128), under the terms of the Creative Commons Attribution License 4.0 (CCBY). AD, Alzheimer's disease; CN, control; GMV, grey matter volume; MWF, myelin water fraction; T1W, T1-weighted; WMV, white matter volume.

selectively with the IR-based UTE (IR-TUE) sequences. The short repetition time adiabatic IR UTE (STAIR-UTE) sequence allows more efficient suppression of various water components in the brain with a broad range of T1s and T2s. *Figure* 7 shows 3D STAIR-UTE myelin PD maps for a healthy 36-year-old male volunteer (*Figure* 7*A*-7*D*) and a 72-year-old female AD patient (*Figure* 7*E*-7*H*). Normal WM (NWM) in the healthy volunteer has a myelin PD ~9 mol/L, while normal GM (NGM) has a myelin PD ~5 mol/L, largely consistent with the literature. The AD patient shows extensive myelin loss with a myelin PD of ~5–7 mol/L for NAWM.

Artificial intelligence (AI) in AD

AI has played a crucial role in addressing neurological diseases, particularly through the analysis of imaging data. Traditional machine learning (ML) models, including radiomics features, have demonstrated effectiveness in evaluating pathologies (144). Deep learning (DL), a newer approach within ML, employs convolutional neural networks (CNNs) for in-depth analysis of biomedical images.

DL-based networks consist of neurons that perform mathematical operations on input data, aiming to establish relationships between input (e.g., images, clinical data) and output (e.g., disease presence, survival status) data (145). Public datasets such as Alzheimer's Disease Neuroimaging Initiative (ADNI) (146) and Open Access Series of Imaging Studies (OASIS) (147) provide valuable medical image sets for AI applications in AD.

AI has been applied in various aspects of MRI imaging, including image reconstruction, denoising, segmentation, synthesis, disease prediction, and aiding in disease diagnosis and prognosis.

Diagnostic/prognostic analysis

One of the most popular tasks in articles that used AI for AD assessment is classification and AD diagnoses, such as the binary classification of AD *vs.* MCI (148), AD *vs.* normal (149-151), or MCI *vs.* normal, or multi-class classification such as AD *vs.* MCI *vs.* normal (152-154). In this light, Gupta *et al.* (155) utilized the ADNI dataset to classify patients into MCI and AD using a support vector machine (SVM) classifier. In another article, Kam *et al.* (156) made a CNN-based model that detects MCI at an early stage using resting-state functional MRI scans. Cui *et al.* (157) also showed that DL models are capable of classifying patients into AD, MCI, and healthy by analyzing the hippocampus

© AME Publishing Company.

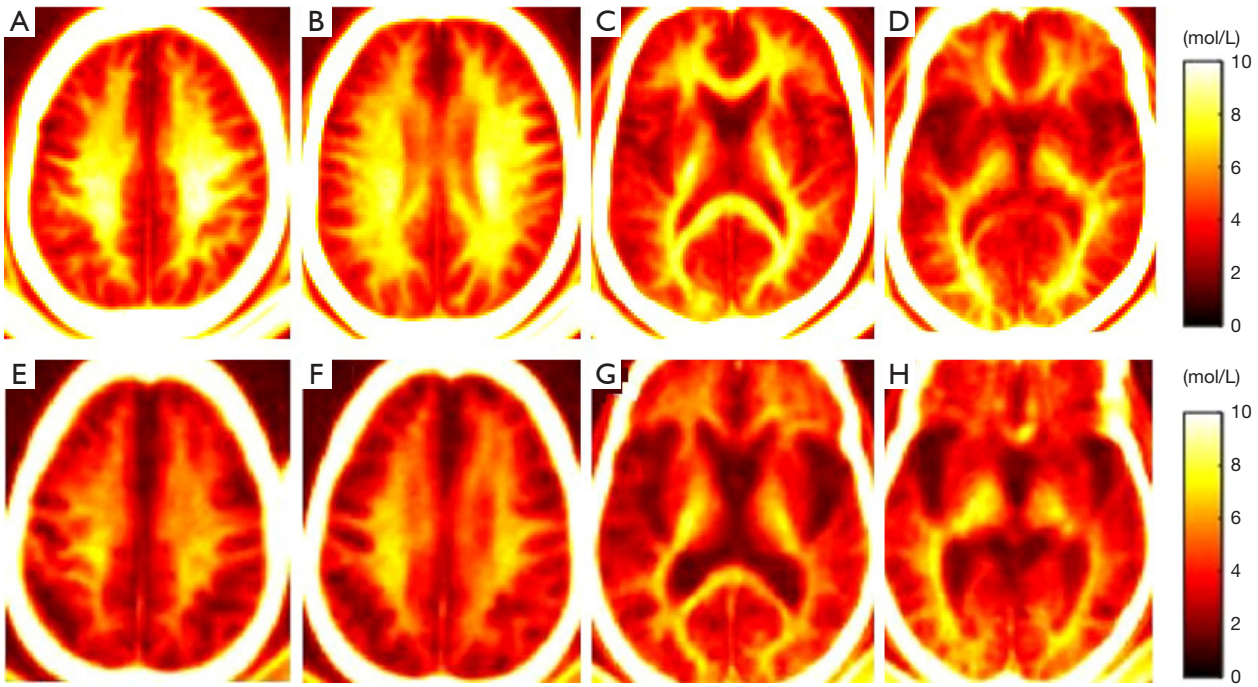

Figure 7 Selected myelin PD maps of a 36-year-old healthy male volunteer (A-D) and a 72-year-old female AD patient (E-H) generated from 3D STAIR-UTE imaging. The AD patient (WM myelin PD ~5–7 mol/L) shows extensive myelin loss across the whole brain compared to the healthy volunteer (WM myelin PD ~8–10 mol/L). AD, Alzheimer's disease; PD, parkinson disease; STAIR, short repetition time adiabatic inversion recovery; UTE, ultrashort echo time; WM, white matter.

and its adjacent areas in T1-weighted MRI scans.

In addition, the identification of progression in MCI and AD patients has always been of interest in the literature (158-160). In a study by Spasov *et al.* (158), researchers trained a neural network model on 785 patients and aimed to predict whether a patient with MCI would proceed to AD or not in the future. Their model achieved AUC of 0.925 which can be considered decent for clinical application. In another study, Fisher *et al.* (159) built and utilized an unsupervised ML model to correctly predict AD progression in 1909 patients. Another research study (160) focused on the development of a recurrent neural network in order to forecast MCI progression into AD, reaching AUCs of 0.83–0.86 and utilizing multi-modal ADNI data.

Image reconstruction & denoising

Traditional reconstruction methods for radiological scans require a considerable amount of time and computation. DL-based models have performed much faster and have simplified complex computation patterns, leading to more accurate and readily available images. For example, DL achieves more efficient and speedier PET (161) and PET/MR (162) reconstructed images of AD patients, which would help when the physician aims for lower acquisition time or the patient cannot cooperate well.

DL has also helped with the denoising task of MRI images. The application of AI models to reconstructed MR images would lead to higher-quality images that contain more informative data and are less blurry or have fewer artifacts. A few studies have utilized AI-based denoising systems in AD (163-165). According to Kanemaru *et al.* (163), the AI denoising system efficiently reduces the noise, keeping the necessary contrast. The study of Lee *et al.* (164) reached the same results using PET images. Last but not least, Ravi *et al.* (165) developed a DL-based denoising system applied to MRI images, achieving high quality images.

Image synthesis

DL models, especially generative adversarial networks (GANs), have emerged as a tool to create synthetic medical images. These models mimic a real-world sample of an image and transform it into a completely synthesized image

© AME Publishing Company.

that cannot be easily distinguished from a true patient image. This helps in the training process of other AI models that need very high numbers of data samples. For example, several research articles have focused on the use of GANs for the aim of MRI image synthesis and applying a classifier to categorize data into AD and normal cases (166). Another instance is the study of Hamghalam *et al.* (167), which utilized GANs to generate new MR images and then fed the images to a DL-based segmentation model. Their final model aimed to segment white and GM, which is also a crucial task for AD.

Segmentation

Image segmentation can be referred to as dividing the image pixels into two or more subgroups. For example, one may try to distinguish WM from GM and/or CSF, which we can refer to as tissue segmentation. Another instance is the separation of the hippocampus from other brain areas, which can be regarded as anatomical segmentation. The latter plays a key role in the analysis of AD as much of the underlying pathology of AD remains in the morphometry analysis of the hippocampal area. Segmentation masks can be achieved using either traditional ML models or novel DL networks such as U-net, which has emerged as one of the fundamental medical imaging segmentation models (168). In this regard, several studies have investigated the use of AI for the segmentation of the hippocampus in MRI data (169,170).

Challenges of AI

There are, however, some challenges imposed with the applicability of AI in AD research. For example, we need larger multi-institutional imaging datasets coupled with demographical, clinical, and genomics features in order to construct a holistic model. Unfortunately, this goal remains hard to reach as several institutions disallow the public share of patients' data. In addition, current research in AI has focused on the development of new models rather than the translation of

currently-developed models to an external dataset. Furthermore, a literature review also shows the lack of globally accepted reporting guidelines to standardize the methodologies of articles, except for some checklists such as Checklist for Artificial Intelligence in Medical Imaging (CLAIM) 32 which is still not widely used in the literature. Addressing these challenges would definitely help establish a better foundation for AI research in AD, leading to more generalizable, explainable, and trustworthy models that will be readily applied to daily clinical practice.

Conclusions

The integration of myelin damage in the understanding of AD pathophysiology has significant implications for both research and clinical practice. Traditionally viewed as a disorder primarily affecting GM, mounting evidence suggests that myelin damage is not only a central feature of AD but may also precede the development of hallmark pathologies such as amyloid-beta (Aβ) plaques and tau tangles. This paradigm shift underscores the importance of WM integrity and myelin preservation in the context of AD.

As described in the review, multiple relaxation components have been described in the brain using T1, T2*, T1ρ, and MT analysis. Although most T1ρ bicomponent research has focused on musculoskeletal tissues such as tendons and cartilage (171-174), demonstrating promising outcomes, its extension to brain analysis highlights the potential for valuable insights into neural relaxation mechanisms. Menon *et al.* (175) demonstrated bi-exponential T1ρ relaxation in brain GM and WM, superior to the traditional single component fitting, providing greater information on bound and free water components. *Table 2* summarises the quantitative imaging biomarkers and their behaviour in AD.

PET is another neuroimaging tool that has been used to quantitatively study the molecular processes in the brain (176,177). PET radioligands bind targets such as amyloid beta (178-180), tau (181) and translocator protein 18 kDA (TSPO) (182). The quantitative assessment of amyloid involves measuring the SUVr in the cortical regions associated with significant amyloid burden. Cortical GM regions, i.e., anterior and posterior cingulate, medial orbital frontal, temporal, and parietal lobes and the precuneus are routinely used for analysis (183). A reference region, which is believed not to accumulate amyloid, is required for SUVr calculations. Regions such as the cerebellar cortex, whole cerebellum, pons, and subcortical WM have been used as reference regions for these calculations (184). Qualitative visual assessments using amyloid PET scans have shown a sensitivity of about 84.6% and a specificity of 38.1% for distinguishing AD patients from healthy controls (185). Improved scan parameters and additional biomarkers have enhanced test accuracy. Although more time-consuming, the quantitative assessment of the global cortex SUVr is considered more accurate, with a sensitivity of 92.3% and a specificity of 90.5% (185). However, amyloid PET positivity

© AME Publishing Company.

Table 2 Quantitative magnetic resonance imaging techniques in AD (143)

Quantitative Biomarker	Principle	Acquisition methods	Changes in AD	Advantage/disadvantage
T1	Differential recovery of longitudinal magnetization	• 3D fast low angle shot • Inversion recovery based EPI sequence • Sy-MRI	• Affected by water, amyloid, iron, myelin among other factors—non specific	• The clinical relevance is limited due to the scarcity of studies, although Sy-MRI appears promising
T1ρ	Spin lattice relaxation time in rotating frame	• Spin lock preparation with varying spin lock times	• Higher dynamic range than T2. • Increased T1ρ values indicate pathology	• High SAR • Relatively fewer studies and longer scan time • Bi-component T1ρ analysis can further expand our understanding of pathology
T2	Decay of transverse magnetization (spin-spin relaxation time)	• T2 quantification using different echo times	• T2 values are affected by iron (reduces T2) and water (increases T2) content	• Most studied biomarker • Widely available, shorter scan times • Susceptible to magic angle effect
QSM	Quantify the spatial distribution of magnetic susceptibility within tissue	• Multiecho gradient echo with post processing: region extraction, phase unwrapping, background field removal, and magnetic dipole inversion	• Negative susceptibility for Beta amyloid and positive susceptibility for iron—colocalization may introduce contrasting effects	• Presence of other ions—copper, calcium, different states of iron could affect QSM values • Limited clinical application
Magnetization transfer imaging	Magnetization exchange between free water and bound water (macromolecular or tightly bound water)	• Using off resonance saturation pulses of different powers and frequencies	• Reduction in MTR in AD brains • MMF can be used to quantify macromolecular (myelin) content and is reduced in regions affected with AD	• Not affected by fiber orientation/magic angle effect • High SAR • Can be used to measure intrinsic tissue properties, e.g., k_{for}
MWF/MPD	Ratio of short T2 (MW distribution) to entire T2 distribution	• mcDESPOT • ViSTa • UTE-STAIR (myelin proton fraction)	• Reduction in MWF and MPD in AD affected areas	• MPD allows for direct myelin imaging

AD, Alzheimer's disease; EPI, echo planar imaging; MTR, magnetization transfer ratio; MMF, macromolecular fraction; MWF, myelin water fraction; MPD, myelin proton density; MW, myelin water; mcDESPOT, multicomponent driven equilibrium steady-state observation of T1 and T2; QSM, quantitative susceptibility mapping; SAR, specific absorption ratio; STAIR, short repetition time adiabatic inversion recovery; Sy-MRI, synthetic magnetic resonance imaging; UTE, ultrashort echo time; ViSTa, direct visualization of short transverse relaxation time component.

is seen in healthy older adults, with amyloid positivity rates ranging from 10–12% in those 60 to 70 years old to more than 50% in persons aged 80–90 years (186). A positive amyloid scan can also be seen in other medical conditions like Lewy body dementia (187). Amyloid PET scans may, in certain instances, underestimate the brain amyloid plaque burden, especially in the setting of low CSF Aβ42 levels (188). In addition, diffusion tensor imaging (DTI) has also been used extensively to study the neurodegeneration in AD and recently used to study early AD changes (189). DTI was not included in our paper because of multiple reviews on DTI in AD in published literature, and also

© AME Publishing Company.

because we wanted to focus on techniques that directly visualize and quantify the myelin content, iron deposition and localized neurodegeneration.

In discussing the challenges surrounding quantitative imaging and integration of AI, several key obstacles emerge. Foremost among these is the time-consuming nature of quantitative imaging techniques, which presents a significant barrier to their widespread adoption in clinical settings. Furthermore, the lack of standardized sequences for different MRI platforms complicates the comparison and reproducibility of results across studies. Current research in AI has focused on developing new models rather than translating currently-developed models to an external dataset. Furthermore, a literature review also shows the lack of globally accepted reporting guidelines to standardize the methodologies of articles, except for some checklists such as CLAIM (190), which is still not widely used in the literature. Addressing this issue is crucial to establishing robust and reliable quantitative imaging protocols.

Additionally, the necessity for large sample sizes in quantitative imaging studies poses logistical and resource challenges, requiring considerable effort to recruit and retain participants. Larger multi-institutional imaging datasets coupled with demographical, clinical, and genomics features are needed to construct holistic AI models. Unfortunately, this goal remains hard to reach as several institutions disallow the public share of patients' data. Moreover, the analysis of quantitative imaging data demands advanced algorithms and computational expertise, underscoring the importance of skilled technicians and researchers in this field. Lastly, as quantitative imaging becomes increasingly utilized in the diagnosis and monitoring of AD, there is a pressing need for further research to differentiate between different pathologies that may overlap with AD. This highlights the complexity inherent in utilizing quantitative imaging as a diagnostic tool and underscores the importance of ongoing investigation to fully realize its potential in clinical practice.

Acknowledgments

None.

Footnote

Reporting Checklist: The authors have completed the Narrative Review reporting checklist. Available at https://qims.amegroups.com/article/view/10.21037/qims-24-1602/rc

Funding: This work was supported by the National Institutes of Health (No. RF1AG075717) and Veterans Affairs Clinical Science Research and Development (No. I01CX002211).

Conflicts of Interest: All authors have completed the ICMJE uniform disclosure form (available at https://qims.amegroups.com/article/view/10.21037/qims-24-1602/coif). J.D. serves as an unpaid editorial board member of *Quantitative Imaging in Medicine and Surgery*. The authors have no conflicts of interest to declare.

Ethical Statement: The authors are accountable for all aspects of the work in ensuring that questions related to the accuracy or integrity of any part of the work are appropriately investigated and resolved. Written informed consent was obtained from each participant as approved by the institutional review board (IRB) of the University of California, San Diego.

Open Access Statement: This is an Open Access article distributed in accordance with the Creative Commons Attribution-NonCommercial-NoDerivs 4.0 International License (CC BY-NC-ND 4.0), which permits the non-commercial replication and distribution of the article with the strict proviso that no changes or edits are made and the original work is properly cited (including links to both the formal publication through the relevant DOI and the license). See: https://creativecommons.org/licenses/by-nc-nd/4.0/.

References

1. 2010 Alzheimer's disease facts and figures. Alzheimers Dement 2010;6:158-94.
2. 2023 Alzheimer's disease facts and figures. Alzheimers Dement 2023;19:1598-695.
3. Qiu C, Kivipelto M, von Strauss E. Epidemiology of Alzheimer's disease: occurrence, determinants, and strategies toward intervention. Dialogues Clin Neurosci 2009;11:111-28.
4. Rajan KB, Weuve J, Barnes LL, McAninch EA, Wilson RS, Evans DA. Population estimate of people with clinical Alzheimer's disease and mild cognitive impairment in the United States (2020-2060). Alzheimers Dement 2021;17:1966-75.
5. Estimates of funding for various Research, Condition, and

Disease categories (RCDC) [Internet]. 2023 31 [cited 2024 Mar 4]. Available online: https://report.nih.gov/funding/categorical-spending#/
6. Brenowitz WD, Nelson PT, Besser LM, Heller KB, Kukull WA. Cerebral amyloid angiopathy and its co-occurrence with Alzheimer's disease and other cerebrovascular neuropathologic changes. Neurobiol Aging 2015;36:2702-8.
7. Jellinger KA. Prevalence and impact of cerebrovascular lesions in Alzheimer and lewy body diseases. Neurodegener Dis 2010;7:112-5.
8. Dallaire-Théroux C, Callahan BL, Potvin O, Saikali S, Duchesne S. Radiological-Pathological Correlation in Alzheimer's Disease: Systematic Review of Antemortem Magnetic Resonance Imaging Findings. J Alzheimers Dis 2017;57:575-601.
9. Dubois B, Feldman HH, Jacova C, Dekosky ST, Barberger-Gateau P, Cummings J, Delacourte A, Galasko D, Gauthier S, Jicha G, Meguro K, O'brien J, Pasquier F, Robert P, Rossor M, Salloway S, Stern Y, Visser PJ, Scheltens P. Research criteria for the diagnosis of Alzheimer's disease: revising the NINCDS-ADRDA criteria. Lancet Neurol 2007;6:734-46.
10. Hyman BT, Trojanowski JQ. Consensus recommendations for the postmortem diagnosis of Alzheimer disease from the National Institute on Aging and the Reagan Institute Working Group on diagnostic criteria for the neuropathological assessment of Alzheimer disease. J Neuropathol Exp Neurol 1997;56:1095-7.
11. Bendlin BB, Carlsson CM, Johnson SC, Zetterberg H, Blennow K, Willette AA, Okonkwo OC, Sodhi A, Ries ML, Birdsill AC, Alexander AL, Rowley HA, Puglielli L, Asthana S, Sager MA. CSF T-Tau/Aβ42 predicts white matter microstructure in healthy adults at risk for Alzheimer's disease. PLoS One 2012;7:e37720.
12. Papuć E, Rejdak K. The role of myelin damage in Alzheimer's disease pathology. Arch Med Sci 2020;16:345-51.
13. Couttas TA, Kain N, Suchowerska AK, Quek LE, Turner N, Fath T, Garner B, Don AS. Loss of ceramide synthase 2 activity, necessary for myelin biosynthesis, precedes tau pathology in the cortical pathogenesis of Alzheimer's disease. Neurobiol Aging 2016;43:89-100.
14. Desai MK, Sudol KL, Janelsins MC, Mastrangelo MA, Frazer ME, Bowers WJ. Triple-transgenic Alzheimer's disease mice exhibit region-specific abnormalities in brain myelination patterns prior to appearance of amyloid and tau pathology. Glia 2009;57:54-65.
15. Stokin GB, Lillo C, Falzone TL, Brusch RG, Rockenstein E, Mount SL, Raman R, Davies P, Masliah E, Williams DS, Goldstein LS. Axonopathy and transport deficits early in the pathogenesis of Alzheimer's disease. Science 2005;307:1282-8.
16. Bartzokis G, Sultzer D, Lu PH, Nuechterlein KH, Mintz J, Cummings JL. Heterogeneous age-related breakdown of white matter structural integrity: implications for cortical "disconnection" in aging and Alzheimer's disease. Neurobiol Aging 2004;25:843-51.
17. Bartzokis G, Lu PH, Mintz J. Human brain myelination and amyloid beta deposition in Alzheimer's disease. Alzheimers Dement 2007;3:122-5.
18. Liao MC, Ahmed M, Smith SO, Van Nostrand WE. Degradation of amyloid beta protein by purified myelin basic protein. J Biol Chem 2009;284:28917-25.
19. Quintela-López T, Ortiz-Sanz C, Serrano-Regal MP, Gaminde-Blasco A, Valero J, Baleriola J, Sánchez-Gómez MV, Matute C, Alberdi E. Aβ oligomers promote oligodendrocyte differentiation and maturation via integrin β1 and Fyn kinase signaling. Cell Death Dis 2019;10:445.
20. Horiuchi M, Maezawa I, Itoh A, Wakayama K, Jin LW, Itoh T, Decarli C. Amyloid β1-42 oligomer inhibits myelin sheet formation in vitro. Neurobiol Aging 2012;33:499-509.
21. Lee JT, Xu J, Lee JM, Ku G, Han X, Yang DI, Chen S, Hsu CY. Amyloid-beta peptide induces oligodendrocyte death by activating the neutral sphingomyelinase-ceramide pathway. J Cell Biol 2004;164:123-31.
22. Dean DC 3rd, Hurley SA, Kecskemeti SR, O'Grady JP, Canda C, Davenport-Sis NJ, Carlsson CM, Zetterberg H, Blennow K, Asthana S, Sager MA, Johnson SC, Alexander AL, Bendlin BB. Association of Amyloid Pathology With Myelin Alteration in Preclinical Alzheimer Disease. JAMA Neurol 2017;74:41-9.
23. Chandra A, Dervenoulas G, Politis M; Alzheimer's Disease Neuroimaging Initiative. Magnetic resonance imaging in Alzheimer's disease and mild cognitive impairment. J Neurol 2019;266:1293-302.
24. van Oostveen WM, de Lange ECM. Imaging Techniques in Alzheimer's Disease: A Review of Applications in Early Diagnosis and Longitudinal Monitoring. Int J Mol Sci 2021;22:2110.
25. Lombardi G, Crescioli G, Cavedo E, Lucenteforte E, Casazza G, Bellatorre AG, Lista C, Costantino G, Frisoni G, Virgili G, Filippini G. Structural magnetic resonance imaging for the early diagnosis of dementia due to Alzheimer's disease in people with mild

© AME Publishing Company.

cognitive impairment. Cochrane Database Syst Rev 2020;3:CD009628.
26. Reiman EM, Jagust WJ. Brain imaging in the study of Alzheimer's disease. Neuroimage 2012;61:505-16.
27. Bozzali M, Serra L, Cercignani M. Quantitative MRI to understand Alzheimer's disease pathophysiology. Curr Opin Neurol 2016;29:437-44.
28. Han L, Jiang H, Yao X, Ren Z, Qu Z, Yu T, Luo S, Wu T. Revealing the correlations between brain cortical characteristics and susceptibility genes for Alzheimer disease: a cross-sectional study. Quant Imaging Med Surg 2023;13:2451-65.
29. Leandrou S, Petroudi S, Kyriacou PA, Reyes-Aldasoro CC, Pattichis CS. Quantitative MRI Brain Studies in Mild Cognitive Impairment and Alzheimer's Disease: A Methodological Review. IEEE Rev Biomed Eng 2018;11:97-111.
30. Knopman DS, DeKosky ST, Cummings JL, Chui H, Corey-Bloom J, Relkin N, Small GW, Miller B, Stevens JC. Practice parameter: diagnosis of dementia (an evidence-based review). Report of the Quality Standards Subcommittee of the American Academy of Neurology. Neurology 2001;56:1143-53.
31. Jack CR Jr, Barkhof F, Bernstein MA, Cantillon M, Cole PE, Decarli C, et al. Steps to standardization and validation of hippocampal volumetry as a biomarker in clinical trials and diagnostic criterion for Alzheimer's disease. Alzheimers Dement 2011;7:474-485.e4.
32. Sørensen L, Igel C, Liv Hansen N, Osler M, Lauritzen M, Rostrup E, Nielsen M; Alzheimer's Disease Neuroimaging Initiative and the Australian Imaging Biomarkers and Lifestyle Flagship Study of Ageing. Early detection of Alzheimer's disease using MRI hippocampal texture. Hum Brain Mapp 2016;37:1148-61.
33. Lee S, Lee H, Kim KW; Alzheimer's Disease Neuroimaging Initiative. Magnetic resonance imaging texture predicts progression to dementia due to Alzheimer disease earlier than hippocampal volume. J Psychiatry Neurosci 2020;45:7-14.
34. Leandrou S, Petroudi S, Kyriacou PA, Reyes-Aldasoro CC, Pattichis CS. An Overview of Quantitative Magnetic Resonance Imaging Analysis Studies in the Assessment of Alzheimer's Disease. In: Kyriacou E, Christofides S, Pattichis CS, editors. XIV Mediterranean Conference on Medical and Biological Engineering and Computing 2016. Cham: Springer International Publishing; 2016:281-6.
35. El Tannir El Tayara N, Delatour B, Le Cudennec C, Guégan M, Volk A, Dhenain M. Age-related evolution of amyloid burden, iron load, and MR relaxation times in a transgenic mouse model of Alzheimer's disease. Neurobiol Dis 2006;22:199-208.
36. House MJ, St Pierre TG, McLean C. 1.4T study of proton magnetic relaxation rates, iron concentrations, and plaque burden in Alzheimer's disease and control postmortem brain tissue. Magn Reson Med 2008;60:41-52.
37. Forster D, Davies K, Williams S. Magnetic resonance spectroscopy in vivo of neurochemicals in a transgenic model of Alzheimer's disease: a longitudinal study of metabolites, relaxation time, and behavioral analysis in TASTPM and wild-type mice. Magn Reson Med 2013;69:944-55.
38. Gouw AA, Seewann A, Vrenken H, van der Flier WM, Rozemuller JM, Barkhof F, Scheltens P, Geurts JJ. Heterogeneity of white matter hyperintensities in Alzheimer's disease: post-mortem quantitative MRI and neuropathology. Brain 2008;131:3286-98.
39. Su L, Blamire AM, Watson R, He J, Aribisala B, O'Brien JT. Cortical and Subcortical Changes in Alzheimer's Disease: A Longitudinal and Quantitative MRI Study. Curr Alzheimer Res 2016;13:534-44.
40. Lou B, Jiang Y, Li C, Wu PY, Li S, Qin B, Chen H, Wang R, Wu B, Chen M. Quantitative Analysis of Synthetic Magnetic Resonance Imaging in Alzheimer's Disease. Front Aging Neurosci 2021;13:638731.
41. Destrieux C, Fischl B, Dale A, Halgren E. Automatic parcellation of human cortical gyri and sulci using standard anatomical nomenclature. Neuroimage 2010;53:1-15.
42. Parent O, Bussy A, Devenyi GA, Dai A, Costantino M, Tullo S, Salaciak A, Bedford S, Farzin S, Béland ML, Valiquette V, Villeneuve S, Poirier J, Tardif CL, Dadar M; Chakravarty MM. Assessment of white matter hyperintensity severity using multimodal magnetic resonance imaging. Brain Commun 2023;5:fcad279.
43. Yuan J, Wang YXJ. T1rho MR Imaging: Principle, Technology, and Application. In: Farncombe T, Iniewski K, editors. Medical Imaging. CRC Press; 2014.
44. Borthakur A, Wheaton AJ, Gougoutas AJ, Akella SV, Regatte RR, Charagundla SR, Reddy R. In vivo measurement of T1rho dispersion in the human brain at 1.5 tesla. J Magn Reson Imaging 2004;19:403-9.
45. Borthakur A, Sochor M, Davatzikos C, Trojanowski JQ, Clark CM. T1rho MRI of Alzheimer's disease. Neuroimage 2008;41:1199-205.
46. Haris M, Singh A, Cai K, Davatzikos C, Trojanowski JQ, Melhem ER, Clark CM, Borthakur A. T1rho (T1ρ) MR imaging in Alzheimer's disease and Parkinson's disease

© AME Publishing Company.

with and without dementia. J Neurol 2011;258:380-5.
47. Haris M, Yadav SK, Rizwan A, Singh A, Cai K, Kaura D, Wang E, Davatzikos C, Trojanowski JQ, Melhem ER, Marincola FM, Borthakur A. T1rho MRI and CSF biomarkers in diagnosis of Alzheimer's disease. Neuroimage Clin 2015;7:598-604.
48. Kettunen MI, Gröhn OH, Silvennoinen MJ, Penttonen M, Kauppinen RA. Effects of intracellular pH, blood, and tissue oxygen tension on T1rho relaxation in rat brain. Magn Reson Med 2002;48:470-7.
49. Magnotta VA, Heo HY, Dlouhy BJ, Dahdaleh NS, Follmer RL, Thedens DR, Welsh MJ, Wemmie JA. Detecting activity-evoked pH changes in human brain. Proc Natl Acad Sci U S A 2012;109:8270-3.
50. Jokivarsi KT, Hiltunen Y, Gröhn H, Tuunanen P, Gröhn OH, Kauppinen RA. Estimation of the onset time of cerebral ischemia using T1rho and T2 MRI in rats. Stroke 2010;41:2335-40.
51. Kettunen MI, Sierra A, Närväinen MJ, Valonen PK, Ylä-Herttuala S, Kauppinen RA, Gröhn OH. Low spin-lock field T1 relaxation in the rotating frame as a sensitive MR imaging marker for gene therapy treatment response in rat glioma. Radiology 2007;243:796-803.
52. Boles Ponto LL, Magnotta VA, Menda Y, Moser DJ, Oleson JJ, Harlynn EL, DeVries SD, Wemmie JA, Schultz SK. Comparison of T(1)Rho MRI, Glucose Metabolism, and Amyloid Burden Across the Cognitive Spectrum: A Pilot Study. J Neuropsychiatry Clin Neurosci 2020;32:352-61.
53. Wang L, Chen W, Qian Y, So TY. Repeatability of quantitative T1rho magnetic resonance imaging in normal brain tissues at 3.0T. Phys Med 2023;112:102641.
54. Kirsch SJ, Jacobs RW, Butcher LL, Beatty J. Prolongation of magnetic resonance T2 time in hippocampus of human patients marks the presence and severity of Alzheimer's disease. Neurosci Lett 1992;134:187-90.
55. Laakso MP, Partanen K, Soininen H, Lehtovirta M, Hallikainen M, Hänninen T, Helkala EL, Vainio P, Riekkinen PJ Sr. MR T2 relaxometry in Alzheimer's disease and age-associated memory impairment. Neurobiol Aging 1996;17:535-40.
56. Pitkänen A, Laakso M, Kälviäinen R, Partanen K, Vainio P, Lehtovirta M, Riekkinen P, Soininen H. Severity of hippocampal atrophy correlates with the prolongation of MRI T2 relaxation time in temporal lobe epilepsy but not in Alzheimer's disease. Neurology 1996;46:1724-30.
57. Wang H, Yuan H, Shu L, Xie J, Zhang D. Prolongation of T(2) relaxation times of hippocampus and amygdala in Alzheimer's disease. Neurosci Lett 2004;363:150-3.
58. Raven EP, Lu PH, Tishler TA, Heydari P, Bartzokis G. Increased iron levels and decreased tissue integrity in hippocampus of Alzheimer's disease detected in vivo with magnetic resonance imaging. J Alzheimers Dis 2013;37:127-36.
59. Vickers JC, Mitew S, Woodhouse A, Fernandez-Martos CM, Kirkcaldie MT, Canty AJ, McCormack GH, King AE. Defining the earliest pathological changes of Alzheimer's disease. Curr Alzheimer Res 2016;13:281-7.
60. Rao YL, Ganaraja B, Murlimanju BV, Joy T, Krishnamurthy A, Agrawal A. Hippocampus and its involvement in Alzheimer's disease: a review. 3 Biotech 2022;12:55.
61. Haley AP, Knight-Scott J, Fuchs KL, Simnad VI, Manning CA. Shortening of hippocampal spin-spin relaxation time in probable Alzheimer's disease: a 1H magnetic resonance spectroscopy study. Neurosci Lett 2004;362:167-70.
62. Luo Z, Zhuang X, Kumar D, Wu X, Yue C, Han C, Lv J. The correlation of hippocampal T2-mapping with neuropsychology test in patients with Alzheimer's disease. PLoS One 2013;8:e76203.
63. Tran D, DiGiacomo P, Born DE, Georgiadis M, Zeineh M. Iron and Alzheimer's Disease: From Pathology to Imaging. Front Hum Neurosci 2022;16:838692.
64. Ayton S, Portbury S, Kalinowski P, Agarwal P, Diouf I, Schneider JA, Morris MC, Bush AI. Regional brain iron associated with deterioration in Alzheimer's disease: A large cohort study and theoretical significance. Alzheimers Dement 2021;17:1244-56.
65. Hagemeier J, Geurts JJ, Zivadinov R. Brain iron accumulation in aging and neurodegenerative disorders. Expert Rev Neurother 2012;12:1467-80.
66. Grundke-Iqbal I, Fleming J, Tung YC, Lassmann H, Iqbal K, Joshi JG. Ferritin is a component of the neuritic (senile) plaque in Alzheimer dementia. Acta Neuropathol 1990;81:105-10.
67. Schubert D, Chevion M. The role of iron in beta amyloid toxicity. Biochem Biophys Res Commun 1995;216:702-7.
68. Bishop GM, Robinson SR. Human Abeta1-42 reduces iron-induced toxicity in rat cerebral cortex. J Neurosci Res 2003;73:316-23.
69. Good PF, Perl DP, Bierer LM, Schmeidler J. Selective accumulation of aluminum and iron in the neurofibrillary tangles of Alzheimer's disease: a laser microprobe (LAMMA) study. Ann Neurol 1992;31:286-92.
70. Smith MA, Harris PL, Sayre LM, Perry G. Iron accumulation in Alzheimer disease is a source of redox-

© AME Publishing Company.

generated free radicals. Proc Natl Acad Sci U S A 1997;94:9866-8.
71. Schenck JF, Zimmerman EA, Li Z, Adak S, Saha A, Tandon R, Fish KM, Belden C, Gillen RW, Barba A, Henderson DL, Neil W, O'Keefe T. High-field magnetic resonance imaging of brain iron in Alzheimer disease. Top Magn Reson Imaging 2006;17:41-50.
72. Schweser F, Deistung A, Reichenbach JR. Foundations of MRI phase imaging and processing for Quantitative Susceptibility Mapping (QSM). Z Med Phys 2016;26:6-34.
73. Crielaard BJ, Lammers T, Rivella S. Targeting iron metabolism in drug discovery and delivery. Nat Rev Drug Discov 2017;16:400-23.
74. Kawahara M, Kato-Negishi M, Tanaka K. Cross talk between neurometals and amyloidogenic proteins at the synapse and the pathogenesis of neurodegenerative diseases. Metallomics 2017;9:619-33.
75. Duce JA, Tsatsanis A, Cater MA, James SA, Robb E, Wikhe K, et al. Iron-export ferroxidase activity of β-amyloid precursor protein is inhibited by zinc in Alzheimer's disease. Cell 2010;142:857-67.
76. Li X, Lei P, Tuo Q, Ayton S, Li QX, Moon S, Volitakis I, Liu R, Masters CL, Finkelstein DI, Bush AI. Enduring Elevations of Hippocampal Amyloid Precursor Protein and Iron Are Features of β-Amyloid Toxicity and Are Mediated by Tau. Neurotherapeutics 2015;12:862-73.
77. Lei P, Ayton S, Finkelstein DI, Spoerri L, Ciccotosto GD, Wright DK, Wong BX, Adlard PA, Cherny RA, Lam LQ, Roberts BR, Volitakis I, Egan GF, McLean CA, Cappai R, Duce JA, Bush AI. Tau deficiency induces parkinsonism with dementia by impairing APP-mediated iron export. Nat Med 2012;18:291-5.
78. Tuo QZ, Lei P, Jackman KA, Li XL, Xiong H, Li XL, et al. Tau-mediated iron export prevents ferroptotic damage after ischemic stroke. Mol Psychiatry 2017;22:1520-30.
79. Uchida Y, Kan H, Sakurai K, Oishi K, Matsukawa N. Contributions of blood-brain barrier imaging to neurovascular unit pathophysiology of Alzheimer's disease and related dementias. Front Aging Neurosci 2023;15:1111448.
80. Uchida Y, Kan H, Furukawa G, Onda K, Sakurai K, Takada K, Matsukawa N, Oishi K. Relationship between brain iron dynamics and blood-brain barrier function during childhood: a quantitative magnetic resonance imaging study. Fluids Barriers CNS 2023;20:60.
81. Uchida Y, Kan H, Sakurai K, Horimoto Y, Hayashi E, Iida A, Okamura N, Oishi K, Matsukawa N. APOE 4 dose associates with increased brain iron and β-amyloid via blood-brain barrier dysfunction. J Neurol Neurosurg Psychiatry 2022. [Epub ahead of print]. doi: 10.1136/jnnp-2021-328519.
82. Uchida Y, Kan H, Sakurai K, Oishi K, Matsukawa N. Quantitative susceptibility mapping as an imaging biomarker for Alzheimer's disease: The expectations and limitations. Front Neurosci 2022;16:938092.
83. Acosta-Cabronero J, Williams GB, Cardenas-Blanco A, Arnold RJ, Lupson V, Nestor PJ. In vivo quantitative susceptibility mapping (QSM) in Alzheimer's disease. PLoS One 2013;8:e81093.
84. Moon Y, Han SH, Moon WJ. Patterns of Brain Iron Accumulation in Vascular Dementia and Alzheimer's Dementia Using Quantitative Susceptibility Mapping Imaging. J Alzheimers Dis 2016;51:737-45.
85. Kim HG, Park S, Rhee HY, Lee KM, Ryu CW, Rhee SJ, Lee SY, Wang Y, Jahng GH. Quantitative susceptibility mapping to evaluate the early stage of Alzheimer's disease. Neuroimage Clin 2017;16:429-38.
86. Gong NJ, Dibb R, Bulk M, van der Weerd L, Liu C. Imaging beta amyloid aggregation and iron accumulation in Alzheimer's disease using quantitative susceptibility mapping MRI. Neuroimage 2019;191:176-85.
87. Cogswell PM, Wiste HJ, Senjem ML, Gunter JL, Weigand SD, Schwarz CG, Arani A, Therneau TM, Lowe VJ, Knopman DS, Botha H, Graff-Radford J, Jones DT, Kantarci K, Vemuri P, Boeve BF, Mielke MM, Petersen RC, Jack CR Jr. Associations of quantitative susceptibility mapping with Alzheimer's disease clinical and imaging markers. Neuroimage 2021;224:117433.
88. Hanyu H, Asano T, Iwamoto T, Takasaki M, Shindo H, Abe K. Magnetization transfer measurements of the hippocampus in patients with Alzheimer's disease, vascular dementia, and other types of dementia. AJNR Am J Neuroradiol 2000;21:1235-42.
89. Hanyu H, Asano T, Sakurai H, Takasaki M, Shindo H, Abe K. Magnetization transfer measurements of the hippocampus in the early diagnosis of Alzheimer's disease. J Neurol Sci 2001;188:79-84.
90. Kabani NJ, Sled JG, Chertkow H. Magnetization transfer ratio in mild cognitive impairment and dementia of Alzheimer's type. Neuroimage 2002;15:604-10.
91. van der Flier WM, van den Heuvel DM, Weverling-Rijnsburger AW, Bollen EL, Westendorp RG, van Buchem MA, Middelkoop HA. Magnetization transfer imaging in normal aging, mild cognitive impairment, and Alzheimer's disease. Ann Neurol 2002;52:62-7.
92. Bozzali M, Franceschi M, Falini A, Pontesilli S,

© AME Publishing Company.

Cercignani M, Magnani G, Scotti G, Comi G, Filippi M. Quantification of tissue damage in AD using diffusion tensor and magnetization transfer MRI. Neurology 2001;57:1135-7.
93. Ridha BH, Symms MR, Tozer DJ, Stockton KC, Frost C, Siddique MM, Lewis EB, MacManus DG, Boulby PA, Barker GJ, Rossor MN, Fox NC, Tofts PS. Magnetization transfer ratio in Alzheimer disease: comparison with volumetric measurements. AJNR Am J Neuroradiol 2007;28:965-70.
94. Ropele S, Schmidt R, Enzinger C, Windisch M, Martinez NP, Fazekas F. Longitudinal magnetization transfer imaging in mild to severe Alzheimer disease. AJNR Am J Neuroradiol 2012;33:570-5.
95. de Jong LW, van der Hiele K, Veer IM, Houwing JJ, Westendorp RG, Bollen EL, de Bruin PW, Middelkoop HA, van Buchem MA, van der Grond J. Strongly reduced volumes of putamen and thalamus in Alzheimer's disease: an MRI study. Brain 2008;131:3277-85.
96. Selden N, Geula C, Hersh L, Mesulam MM. Human striatum: chemoarchitecture of the caudate nucleus, putamen and ventral striatum in health and Alzheimer's disease. Neuroscience 1994;60:621-36.
97. Ryan NS, Keihaninejad S, Shakespeare TJ, Lehmann M, Crutch SJ, Malone IB, Thornton JS, Mancini L, Hyare H, Yousry T, Ridgway GR, Zhang H, Modat M, Alexander DC, Rossor MN, Ourselin S, Fox NC. Magnetic resonance imaging evidence for presymptomatic change in thalamus and caudate in familial Alzheimer's disease. Brain 2013;136:1399-414.
98. de Jong LW, Ferrarini L, van der Grond J, Milles JR, Reiber JH, Westendorp RG, Bollen EL, Middelkoop HA, van Buchem MA. Shape abnormalities of the striatum in Alzheimer's disease. J Alzheimers Dis 2011;23:49-59.
99. Fornari E, Maeder P, Meuli R, Ghika J, Knyazeva MG. Demyelination of superficial white matter in early Alzheimer's disease: a magnetization transfer imaging study. Neurobiol Aging 2012;33:428.e7-19.
100. Giulietti G, Bozzali M, Figura V, Spanò B, Perri R, Marra C, Lacidogna G, Giubilei F, Caltagirone C, Cercignani M. Quantitative magnetization transfer provides information complementary to grey matter atrophy in Alzheimer's disease brains. Neuroimage 2012;59:1114-22.
101. Makovac E, Serra L, Di Domenico C, Marra C, Caltagirone C, Cercignani M, Bozzali M. Quantitative Magnetization Transfer of White Matter Tracts Correlates with Diffusion Tensor Imaging Indices in Predicting the Conversion from Mild Cognitive Impairment to Alzheimer's Disease. J Alzheimers Dis 2018;63:561-75.
102. Duan W, Sehrawat P, Zhou TD, Becker JT, Lopez OL, Gach HM, Dai W. Pattern of Altered Magnetization Transfer Rate in Alzheimer's Disease. J Alzheimers Dis 2022;88:693-705.
103. Zhang X, Ma YJ, Wei Z, Wu M, Ashir A, Jerban S, Li S, Chang EY, Du J. Macromolecular fraction (MMF) from 3D ultrashort echo time cones magnetization transfer (3D UTE-Cones-MT) imaging predicts meniscal degeneration and knee osteoarthritis. Osteoarthritis Cartilage 2021;29:1173-80.
104. Xue YP, Ma YJ, Wu M, Jerban S, Wei Z, Chang EY, Du J. Quantitative 3D Ultrashort Echo Time Magnetization Transfer Imaging for Evaluation of Knee Cartilage Degeneration In Vivo. J Magn Reson Imaging 2021;54:1294-302.
105. Jerban S, Kasibhatla A, Ma Y, Wu M, Chen Y, Guo T, Wan L, Szeverenyi N, Chang EY, Du J. Detecting Articular Cartilage and Meniscus Deformation Effects Using Magnetization Transfer Ultrashort Echo Time (MT-UTE) Modeling during Mechanical Load Application: Ex Vivo Feasibility Study. Cartilage 2021;13:665S-73S.
106. van Gelderen P, Jiang X, Duyn JH. Rapid measurement of brain macromolecular proton fraction with transient saturation transfer MRI. Magn Reson Med 2017;77:2174-85.
107. Yarnykh VL, Bowen JD, Samsonov A, Repovic P, Mayadev A, Qian P, Gangadharan B, Keogh BP, Maravilla KR, Jung Henson LK. Fast whole-brain three-dimensional macromolecular proton fraction mapping in multiple sclerosis. Radiology 2015;274:210-20.
108. Jerban S, Ma Y, Afsahi AM, Lombardi A, Wei Z, Shen M, Wu M, Le N, Chang DG, Chung CB, Du J, Chang EY. Lower Macromolecular Content in Tendons of Female Patients with Osteoporosis versus Patients with Osteopenia Detected by Ultrashort Echo Time (UTE) MRI. Diagnostics (Basel) 2022.
109. Ashir A, Ma Y, Jerban S, Jang H, Wei Z, Le N, Du J, Chang EY. Rotator Cuff Tendon Assessment in Symptomatic and Control Groups Using Quantitative MRI. J Magn Reson Imaging 2020;52:864-72.
110. Song SK, Sun SW, Ramsbottom MJ, Chang C, Russell J, Cross AH. Dysmyelination revealed through MRI as increased radial (but unchanged axial) diffusion of water. Neuroimage 2002;17:1429-36.
111. Underhill HR, Yuan C, Yarnykh VL. Direct quantitative comparison between cross-relaxation imaging and diffusion tensor imaging of the human brain at 3.0 T. Neuroimage

© AME Publishing Company.

2009;47:1568-78.
112. Wheeler-Kingshott CAM, Cercignani M. About "axial" and "radial" diffusivities. Magn Reson Med 2009;61:1255-60.
113. Stikov N, Perry LM, Mezer A, Rykhlevskaia E, Wandell BA, Pauly JM, Dougherty RF. Bound pool fractions complement diffusion measures to describe white matter micro and macrostructure. Neuroimage 2011;54:1112-21.
114. Anisimov NV, Pavlova OS, Pirogov YA, Yarnykh VL. Three-dimensional fast single-point macromolecular proton fraction mapping of the human brain at 0.5 Tesla. Quant Imaging Med Surg 2020;10:1441-9.
115. Naumova AV, Akulov AE, Khodanovich MY, Yarnykh VL. High-resolution three-dimensional macromolecular proton fraction mapping for quantitative neuroanatomical imaging of the rodent brain in ultra-high magnetic fields. Neuroimage 2017;147:985-93.
116. Kiefer C, Brockhaus L, Cattapan-Ludewig K, Ballinari P, Burren Y, Schroth G, Wiest R. Multi-parametric classification of Alzheimer's disease and mild cognitive impairment: the impact of quantitative magnetization transfer MR imaging. Neuroimage 2009;48:657-67.
117. Mole JP, Fasano F, Evans J, Sims R, Hamilton DA, Kidd E, Metzler-Baddeley C. Genetic risk of dementia modifies obesity effects on white matter myelin in cognitively healthy adults. Neurobiol Aging 2020;94:298-310.
118. Mole JP, Fasano F, Evans J, Sims R, Kidd E, Aggleton JP, Metzler-Baddeley C. APOE-ε4-related differences in left thalamic microstructure in cognitively healthy adults. Sci Rep 2020;10:19787.
119. MacKay AL, Laule C. Magnetic Resonance of Myelin Water: An in vivo Marker for Myelin. Brain Plast 2016;2:71-91.
120. Lee J, Hyun JW, Lee J, Choi EJ, Shin HG, Min K, Nam Y, Kim HJ, Oh SH. So You Want to Image Myelin Using MRI: An Overview and Practical Guide for Myelin Water Imaging. J Magn Reson Imaging 2021;53:360-73.
121. Labadie C, Lee JH, Rooney WD, Jarchow S, Aubert-Frécon M, Springer CS Jr, Möller HE. Myelin water mapping by spatially regularized longitudinal relaxographic imaging at high magnetic fields. Magn Reson Med 2014;71:375-87.
122. Prasloski T, Rauscher A, MacKay AL, Hodgson M, Vavasour IM, Laule C, Mädler B. Rapid whole cerebrum myelin water imaging using a 3D GRASE sequence. Neuroimage 2012;63:533-9.
123. Oh J, Han ET, Pelletier D, Nelson SJ. Measurement of in vivo multi-component T2 relaxation times for brain tissue using multi-slice T2 prep at 1.5 and 3 T. Magn Reson Imaging 2006;24:33-43.
124. Oh J, Han ET, Lee MC, Nelson SJ, Pelletier D. Multislice brain myelin water fractions at 3T in multiple sclerosis. J Neuroimaging 2007;17:156-63.
125. Whittall KP, MacKay AL. Quantitative interpretation of NMR relaxation data. Journal of Magnetic Resonance (1969) 1989;84:134-52.
126. Raj A, Pandya S, Shen X, LoCastro E, Nguyen TD, Gauthier SA. Multi-compartment T2 relaxometry using a spatially constrained multi-Gaussian model. PLoS One 2014;9:e98391.
127. Laule C, Leung E, Lis DK, Traboulsee AL, Paty DW, MacKay AL, Moore GR. Myelin water imaging in multiple sclerosis: quantitative correlations with histopathology. Mult Scler 2006;12:747-53.
128. Lim SH, Lee J, Jung S, Kim B, Rhee HY, Oh SH, Park S, Cho AR, Ryu CW, Jahng GH. Myelin-Weighted Imaging Presents Reduced Apparent Myelin Water in Patients with Alzheimer's Disease. Diagnostics (Basel) 2022.
129. Kavroulakis E, Simos PG, Kalaitzakis G, Maris TG, Karageorgou D, Zaganas I, Panagiotakis S, Basta M, Vgontzas A, Papadaki E. Myelin content changes in probable Alzheimer's disease and mild cognitive impairment: Associations with age and severity of neuropsychiatric impairment. J Magn Reson Imaging 2018;47:1359-72.
130. Park M, Lee HP, Kim J, Kim DH, Moon Y, Moon WJ. Brain myelin water fraction is associated with APOE4 allele status in patients with cognitive impairment. J Neuroimaging 2022;32:521-9.
131. van der Knaap MS, Valk J, editors. Myelin and White Matter. In: Magnetic Resonance of Myelination and Myelin Disorders. Berlin, Heidelberg: Springer; 2005:1-19.
132. Waldman A, Rees JH, Brock CS, Robson MD, Gatehouse PD, Bydder GM. MRI of the brain with ultra-short echo-time pulse sequences. Neuroradiology 2003;45:887-92.
133. Horch RA, Gore JC, Does MD. Origins of the ultrashort-T2 1H NMR signals in myelinated nerve: a direct measure of myelin content? Magn Reson Med 2011;66:24-31.
134. Wilhelm MJ, Ong HH, Wehrli SL, Li C, Tsai PH, Hackney DB, Wehrli FW. Direct magnetic resonance detection of myelin and prospects for quantitative imaging of myelin density. Proc Natl Acad Sci U S A 2012;109:9605-10.
135. Du J, Ma G, Li S, Carl M, Szeverenyi NM, VandenBerg S,

© AME Publishing Company.

Corey-Bloom J, Bydder GM. Ultrashort echo time (UTE) magnetic resonance imaging of the short T2 components in white matter of the brain using a clinical 3T scanner. Neuroimage 2014;87:32-41.
136. Du J, Sheth V, He Q, Carl M, Chen J, Corey-Bloom J, Bydder GM. Measurement of T1 of the ultrashort T2* components in white matter of the brain at 3T. PLoS One 2014;9:e103296.
137. Sheth V, Shao H, Chen J, Vandenberg S, Corey-Bloom J, Bydder GM, Du J. Magnetic resonance imaging of myelin using ultrashort Echo time (UTE) pulse sequences: Phantom, specimen, volunteer and multiple sclerosis patient studies. Neuroimage 2016;136:37-44.
138. Ma YJ, Jang H, Chang EY, Hiniker A, Head BP, Lee RR, Corey-Bloom J, Bydder GM, Du J. Ultrashort echo time (UTE) magnetic resonance imaging of myelin: technical developments and challenges. Quant Imaging Med Surg 2020;10:1186-203.
139. Ma YJ, Jang H, Wei Z, Cai Z, Xue Y, Lee RR, Chang EY, Bydder GM, Corey-Bloom J, Du J. Myelin Imaging in Human Brain Using a Short Repetition Time Adiabatic Inversion Recovery Prepared Ultrashort Echo Time (STAIR-UTE) MRI Sequence in Multiple Sclerosis. Radiology 2020;297:392-404.
140. Ma YJ, Jang H, Wei Z, Wu M, Chang EY, Corey-Bloom J, Bydder GM, Du J. Brain ultrashort T(2) component imaging using a short TR adiabatic inversion recovery prepared dual-echo ultrashort TE sequence with complex echo subtraction (STAIR-dUTE-ES). J Magn Reson 2021;323:106898.
141. Ma YJ, Searleman AC, Jang H, Wong J, Chang EY, Corey-Bloom J, Bydder GM, Du J. Whole-Brain Myelin Imaging Using 3D Double-Echo Sliding Inversion Recovery Ultrashort Echo Time (DESIRE UTE) MRI. Radiology 2020;294:362-74.
142. Ma YJ, Searleman AC, Jang H, Fan SJ, Wong J, Xue Y, Cai Z, Chang EY, Corey-Bloom J, Du J. Volumetric imaging of myelin in vivo using 3D inversion recovery-prepared ultrashort echo time cones magnetic resonance imaging. NMR Biomed 2020;33:e4326.
143. Fan SJ, Ma Y, Zhu Y, Searleman A, Szeverenyi NM, Bydder GM, Du J. Yet more evidence that myelin protons can be directly imaged with UTE sequences on a clinical 3T scanner: Bicomponent T2* analysis of native and deuterated ovine brain specimens. Magn Reson Med 2018;80:538-47.
144. Fiani B, Pasko KBD, Sarhadi K, Covarrubias C. Current uses, emerging applications, and clinical integration of artificial intelligence in neuroradiology. Rev Neurosci 2022;33:383-95.
145. Kaka H, Zhang E, Khan N. Artificial Intelligence and Deep Learning in Neuroradiology: Exploring the New Frontier. Can Assoc Radiol J 2021;72:35-44.
146. Jack CR Jr, Bernstein MA, Fox NC, Thompson P, Alexander G, Harvey D, et al. The Alzheimer's Disease Neuroimaging Initiative (ADNI): MRI methods. J Magn Reson Imaging 2008;27:685-91.
147. Marcus DS, Fotenos AF, Csernansky JG, Morris JC, Buckner RL. Open access series of imaging studies: longitudinal MRI data in nondemented and demented older adults. J Cogn Neurosci 2010;22:2677-84.
148. Lu D, Popuri K, Ding GW, Balachandar R, Beg MF; Alzheimer's Disease Neuroimaging Initiative. Multimodal and Multiscale Deep Neural Networks for the Early Diagnosis of Alzheimer's Disease using structural MR and FDG-PET images. Sci Rep 2018;8:5697.
149. Aderghal K, Khvostikov A, Krylov A, Benois-Pineau J, Afdel K, Catheline G. Classification of Alzheimer Disease on Imaging Modalities with Deep CNNs Using Cross-Modal Transfer Learning. In: 2018 IEEE 31st International Symposium on Computer-Based Medical Systems (CBMS); 2018:345-50.
150. Ahmed S, Choi KY, Lee JJ, Kim BC, Kwon GR, Lee KH, Jung HY. Ensembles of Patch-Based Classifiers for Diagnosis of Alzheimer Diseases. IEEE Access 2019;7:73373-83.
151. Khvostikov A, Aderghal K, Benois-Pineau J, Krylov A, Catheline G. 3D CNN-based classification using sMRI and MD-DTI images for Alzheimer disease studies. 2018. arXiv: 1801.05968.
152. Khan NM, Hon M, Abraham N. Transfer Learning with intelligent training data selection for prediction of Alzheimer's Disease. 2019. arXiv: 1906.01160
153. Lian C, Liu M, Zhang J, Shen D. Hierarchical Fully Convolutional Network for Joint Atrophy Localization and Alzheimer's Disease Diagnosis Using Structural MRI. IEEE Trans Pattern Anal Mach Intell 2020;42:880-93.
154. Liu M, Cheng D, Wang K, Wang Y; Alzheimer's Disease Neuroimaging Initiative. Multi-Modality Cascaded Convolutional Neural Networks for Alzheimer's Disease Diagnosis. Neuroinformatics 2018;16:295-308.
155. Gupta Y, Lama RK, Kwon GR; Alzheimer's Disease Neuroimaging Initiative. Prediction and Classification of Alzheimer's Disease Based on Combined Features From Apolipoprotein-E Genotype, Cerebrospinal Fluid, MR, and FDG-PET Imaging Biomarkers. Front Comput

© AME Publishing Company.

Neurosci 2019;13:72.
156. Kam TE, Zhang H, Jiao Z, Shen D. Deep Learning of Static and Dynamic Brain Functional Networks for Early MCI Detection. IEEE Trans Med Imaging 2020;39:478-87.
157. Cui R, Liu M. Hippocampus Analysis by Combination of 3-D DenseNet and Shapes for Alzheimer's Disease Diagnosis. IEEE J Biomed Health Inform 2019;23:2099-107.
158. Spasov S, Passamonti L, Duggento A, Liò P, Toschi N; Alzheimer's Disease Neuroimaging Initiative. A parameter-efficient deep learning approach to predict conversion from mild cognitive impairment to Alzheimer's disease. Neuroimage 2019;189:276-87.
159. Fisher CK, Smith AM, Walsh JR; Abbott, Alliance for Aging Research, Alzheimer's Association, Alzheimer's Foundation of America, AstraZeneca Pharmaceuticals LP, Bristol-Myers Squibb Company, Critical Path Institute, CHDI Foundation, Inc., Eli Lilly and Company, F. Hoffmann-La Roche Ltd, Forest Research Institute, Genentech, Inc., GlaxoSmithKline, Johnson & Johnson, National Health Council, Novartis Pharmaceuticals Corporation, Parkinson's Action Network, Parkinson's Disease Foundation, Pfizer, Inc., sanofi-aventis. Collaborating Organizations: Clinical Data Interchange Standards Consortium (CDISC), Ephibian, Metrum Institute. Machine learning for comprehensive forecasting of Alzheimer's Disease progression. Sci Rep 2019;9:13622.
160. Lee G, Nho K, Kang B, Sohn KA, Kim D; Alzheimer's Disease Neuroimaging Initiative. Predicting Alzheimer's disease progression using multi-modal deep learning approach. Sci Rep 2019;9:1952.
161. Peng Z, Ni M, Shan H, Lu Y, Li Y, Zhang Y, Pei X, Chen Z, Xie Q, Wang S, Xu XG. Feasibility evaluation of PET scan-time reduction for diagnosing amyloid-β levels in Alzheimer's disease patients using a deep-learning-based denoising algorithm. Comput Biol Med 2021;138:104919.
162. Zhao Y, Guo Q, Zhang Y, Zheng J, Yang Y, Du X, Feng H, Zhang S. Application of Deep Learning for Prediction of Alzheimer's Disease in PET/MR Imaging. Bioengineering (Basel) 2023;10:1120.
163. Kanemaru N, Takao H, Amemiya S, Abe O. The effect of a post-scan processing denoising system on image quality and morphometric analysis. J Neuroradiol 2022;49:205-12.
164. Lee MH, Yun CS, Kim K, Lee Y. Effect of Denoising and Deblurring 18F-Fluorodeoxyglucose Positron Emission Tomography Images on a Deep Learning Model's Classification Performance for Alzheimer's Disease. Metabolites 2022;12:231.
165. Ravi KS, Nandakumar G, Thomas N, Lim M, Qian E, Jimeno MM, Poojar P, Jin Z, Quarterman P, Srinivasan G, Fung M, Vaughan JT Jr, Geethanath S. Accelerated MRI using intelligent protocolling and subject-specific denoising applied to Alzheimer's disease imaging. Front Neuroimaging 2023;2:1072759.
166. Qu C, Zou Y, Ma Y, Chen Q, Luo J, Fan H, Jia Z, Gong Q, Chen T. Diagnostic Performance of Generative Adversarial Network-Based Deep Learning Methods for Alzheimer's Disease: A Systematic Review and Meta-Analysis. Front Aging Neurosci 2022;14:841696.
167. Hamghalam M, Wang T, Lei B. High tissue contrast image synthesis via multistage attention-GAN: Application to segmenting brain MR scans. Neural Netw 2020;132:43-52.
168. Yamanakkanavar N, Choi JY, Lee B. MRI Segmentation and Classification of Human Brain Using Deep Learning for Diagnosis of Alzheimer's Disease: A Survey. Sensors (Basel) 2020;20:3243.
169. Dill V, Franco AR, Pinho MS. Automated methods for hippocampus segmentation: the evolution and a review of the state of the art. Neuroinformatics 2015;13:133-50.
170. Giuliano A, Donatelli G, Cosottini M, Tosetti M, Retico A, Fantacci ME. Hippocampal subfields at ultra high field MRI: An overview of segmentation and measurement methods. Hippocampus 2017;27:481-94.
171. Kijowski R, Wilson JJ, Liu F. Bicomponent ultrashort echo time T2* analysis for assessment of patients with patellar tendinopathy. J Magn Reson Imaging 2017;46:1441-7.
172. Liu J, Nazaran A, Ma Y, Chen H, Zhu Y, Du J, Li S, Zhou Q, Zhao Y. Single- and Bicomponent Analyses of T2∗ Relaxation in Knee Tendon and Ligament by Using 3D Ultrashort Echo Time Cones (UTE Cones) Magnetic Resonance Imaging. Biomed Res Int 2019;2019:8597423.
173. Malhi BS, Moazamian D, Shin SH, Athertya JS, Silva L, Jerban S, Jang H, Chang E, Ma Y, Carl M, Du J. Bi-Exponential 3D UTE-T1ρ Relaxation Mapping of Ex Vivo Human Knee Patellar Tendon at 3T. Bioengineering (Basel) 2024;11:66.
174. Malhi BS, Jang H, Malhi MS, Berry DB, Jerban S. Tendon evaluation with ultrashort Echo Time (UTE) MRI: A Systematic Review. Front Musculoskelet Disord 2024;2:1324050.
175. Menon RG, Sharafi A, Windschuh J, Regatte RR. Bi-exponential 3D-T1ρ mapping of whole brain at 3 T. Sci Rep 2018;8:1176.

© AME Publishing Company.

176. Perron J, Ko JH. Review of Quantitative Methods for the Detection of Alzheimer's Disease with Positron Emission Tomography. Applied Sciences 2022;12:11463.
177. Suppiah S, Didier MA, Vinjamuri S. The Who, When, Why, and How of PET Amyloid Imaging in Management of Alzheimer's Disease-Review of Literature and Interesting Images. Diagnostics (Basel) 2019;9:65.
178. Chiang GC, Mao X, Kang G, Chang E, Pandya S, Vallabhajosula S, Isaacson R, Ravdin LD; Shungu DC. Relationships among Cortical Glutathione Levels, Brain Amyloidosis, and Memory in Healthy Older Adults Investigated In Vivo with (1)H-MRS and Pittsburgh Compound-B PET. AJNR Am J Neuroradiol 2017;38:1130-7.
179. Chiaravalloti A, Castellano AE, Ricci M, Barbagallo G, Sannino P, Ursini F, Karalis G, Schillaci O. Coupled Imaging with [18F]FBB and [18F]FDG in AD Subjects Show a Selective Association Between Amyloid Burden and Cortical Dysfunction in the Brain. Mol Imaging Biol 2018;20:659-66.
180. Ciarmiello A, Tartaglione A, Giovannini E, Riondato M, Giovacchini G, Ferrando O, De Biasi M, Passera C, Carabelli E, Mannironi A, Foppiano F, Alfano B, Mansi L. Amyloid burden identifies neuropsychological phenotypes at increased risk of progression to Alzheimer's disease in mild cognitive impairment patients. Eur J Nucl Med Mol Imaging 2019;46:288-96.
181. Rabinovici GD, Schonhaut D, Baker S, Lazaris A, Ossenkoppele R, Lockhart S, Schöll M, Schwimmer H, Vogel JW, Ayakta N, Rosen H, Miller BL, O'Neil JP, Boxer AL, Jagust WJ. Tau PET with [18F]AV1451 in non-alzheimer's disease neurodegenerative syndromes. Alzheimers Dement 2015;11:268-9.
182. Valotassiou V, Malamitsi J, Papatriantafyllou J, Dardiotis E, Tsougos I, Psimadas D, Alexiou S, Hadjigeorgiou G, Georgoulias P. SPECT and PET imaging in Alzheimer's disease. Ann Nucl Med 2018;32:583-93.
183. Pfefferbaum A, Chanraud S, Pitel AL, Müller-Oehring E, Shankaranarayanan A, Alsop DC, Rohlfing T, Sullivan EV. Cerebral blood flow in posterior cortical nodes of the default mode network decreases with task engagement but remains higher than in most brain regions. Cereb Cortex 2011;21:233-44.
184. Schmidt ME, Chiao P, Klein G, Matthews D, Thurfjell L, Cole PE, Margolin R, Landau S, Foster NL, Mason NS, De Santi S, Suhy J, Koeppe RA, Jagust W; Alzheimer's Disease Neuroimaging Initiative. The influence of biological and technical factors on quantitative analysis of amyloid PET: Points to consider and recommendations for controlling variability in longitudinal data. Alzheimers Dement 2015;11:1050-68.
185. Camus V, Payoux P, Barré L, Desgranges B, Voisin T, Tauber C, et al. Using PET with 18F-AV-45 (florbetapir) to quantify brain amyloid load in a clinical environment. Eur J Nucl Med Mol Imaging 2012;39:621-31.
186. Marcus C, Mena E, Subramaniam RM. Brain PET in the diagnosis of Alzheimer's disease. Clin Nucl Med 2014;39:e413-22; quiz e423-6.
187. Kantarci K, Yang C, Schneider JA, Senjem ML, Reyes DA, Lowe VJ, Barnes LL, Aggarwal NT, Bennett DA, Smith GE, Petersen RC, Jack CR Jr, Boeve BF. Antemortem amyloid imaging and β-amyloid pathology in a case with dementia with Lewy bodies. Neurobiol Aging 2012;33:878-85.
188. Lewczuk P, Matzen A, Blennow K, Parnetti L, Molinuevo JL, Eusebi P, Kornhuber J, Morris JC, Fagan AM. Cerebrospinal Fluid Aβ42/40 Corresponds Better than Aβ42 to Amyloid PET in Alzheimer's Disease. J Alzheimers Dis 2017;55:813-22.
189. Uchida Y, Onda K, Hou Z, Troncoso JC, Mori S, Oishi K. Microstructural Neurodegeneration of the Entorhinal-Hippocampus Pathway along the Alzheimer's Disease Continuum. J Alzheimers Dis 2023;95:1107-17.
190. Mongan J, Moy L, Kahn CE Jr. Checklist for Artificial Intelligence in Medical Imaging (CLAIM): A Guide for Authors and Reviewers. Radiol Artif Intell 2020;2:e200029.

Cite this article as: Malhi BS, Lo J, Toto-Brocchi M, Avval AH, Ma Y, Du J. Quantitative magnetic resonance imaging in Alzheimer's disease: a narrative review. Quant Imaging Med Surg 2025;15(4):3641-3664. doi: 10.21037/qims-24-1602

© AME Publishing Company.